AD-A205 588 DOCUMENTATION PAGE

Form Approved
OMB No. 0704-0188

1b. RESTRICTIVE MARKINGS	
2a. SECURITY CLASSIFICATION AUTHORITY	3. DISTRIBUTION/AVAILABILITY OF REPORT
2b. DECLASSIFICATION/DOWNGRADING SCHEDULE	Approved for public release; distribution is unlimited.

4. PERFORMING ORGANIZATION REPORT NUMBER(S)	5. MONITORING ORGANIZATION REPORT NUMBER(S)
GL-88-2	AFOSR TR. 89-0

6a. NAME OF PERFORMING ORGANIZATION	6b. OFFICE SYMBOL (If applicable)	7a. NAME OF MONITORING ORGANIZATION
Analatom, Inc		AFOSR/NA

6c. ADDRESS (City, State, and ZIP Code)	7b. ADDRESS (City, State, and ZIP Code)
Sunnyvale CA 94089	Building 410, Bolling AFB DC 20332-6448

8a. NAME OF FUNDING/SPONSORING ORGANIZATION	8b. OFFICE SYMBOL (If applicable)	9. PROCUREMENT INSTRUMENT IDENTIFICATION NUMBER
AFOSR/NA	NA	F49620-88-C-0126

8c. ADDRESS (City, State, and ZIP Code)	10. SOURCE OF FUNDING NUMBERS			
Building 410, Bolling AFB DC 20332-6448	PROGRAM ELEMENT NO.	PROJECT NO.	TASK NO.	WORK UNIT ACCESSION NO.
	65502F	3005	A1	

11. TITLE (Include Security Classification)

(U) An Instrument for the Simultaneous Measurement of Velocity, Temperature and Density In Unseeded Air Flows

12. PERSONAL AUTHOR(S)
Gabriel Laufer

13a. TYPE OF REPORT	13b. TIME COVERED	14. DATE OF REPORT (Year, Month, Day)	15. PAGE COUNT
Final Technical	FROM 88/8/1 TO 89/1/31	1989,1,31	64

16. SUPPLEMENTARY NOTATION

17.	COSATI CODES		18. SUBJECT TERMS (Continue on reverse if necessary and identify by block number)
FIELD	GROUP	SUB-GROUP	Laser Diagnostics, Laser-Induced Fluorescence, Velocity Measurement

19. ABSTRACT (Continue on reverse if necessary and identify by block number) Two methods for the measurement of the velocity of hypersonic air flows were evaluated. In the first technique, an ArF laser is used to dissociate atmospheric CO_2 into CO which it then dissociates into atomic carbon in the $C(2^1D)$ state. The atomic carbon is further excited into the $C(3^1P)$ state from which it radiates at 247.8 nm. The fluorescence intensity is proportional to the concentration of the CO molecules. When air flows across the exciting beam it sweeps CO molecules and C atoms out of the interaction volume, thereby reducing the fluorescence intensity. The resultant fluorescence may serve for velocity measurement. The alternative technique uses the Doppler shift experienced by moving O_2 molecules when they absorb the radiation of a Raman shifted ArF laser. A method which allows single pulse measurement was described.

The dependence of both techniques on air temperature, density and laser intensity was evaluated. The carbon velocimetry technique was tested in a preliminary experiment which demonstrated that this technique may not have the necessary sensitivity for wind tunnel applications. On the other hand, the Doppler velocimetry was shown theoretically to have high accuracy. Without correction of the errors in the independent measurement of the temperature and density the accuracy of the Doppler velocimetry can exceed 10% for temperatures less than 1500 K and pressures higher than .01 atm. When correcting for the temperature and density effects the velocity measurement uncertainty can be less than 5%. When the measurement is limited by the shot noise the measurement uncertainty is less than 0.1%.

20. DISTRIBUTION/AVAILABILITY OF ABSTRACT	21. ABSTRACT SECURITY CLASSIFICATION
☒ UNCLASSIFIED/UNLIMITED ☒ SAME AS RPT ☒ OTIC USERS	Unclassified

22a. NAME OF RESPONSIBLE INDIVIDUAL	22b. TELEPHONE (Include Area Code)	22c. OFFICE SYMBOL
Julian M Tishkoff	(202) 767-4935	AFOSR/NA

DD Form 1473, JUN 86   Previous editions are obsolete.   SECURITY CLASSIFICATION OF THIS PAGE

Research Personnel

1.   Gabriel Laufer, Ph.D., Principal Investigator
      Analatom, Inc.
      1183 Bordeaux Drive, Suite #1
      Sunnyvale, CA 94089
      (408) 736-9392

2.   Sokol Ibrani, Ph.D., Research Scientist
      Analatom, Inc.
      1183 Bordeaux Drive, Suite #1
      Sunnyvale, CA 94089
      (408) 736-9392

TABLE OF CONTENTS

LIST OF FIGURES

Fig.11. The photon count difference, N_D, following the excitation of the the $v''(0)$ to $v'(13)$ R13 transition vs. the laser wavelength while the velocity is selected as a free parameter. Velocities are ranging from 100 m/sec to 2000 m/sec in intervals of 100 m/sec.

Fig.12. The variation of N_D with velocity for temperatures ranging from 100 K to 1500 K. The laser wavelength is $\lambda = 193.1272$ nm.

Fig.13. Temperature and density corrected FD, $N_D = N_D/N_c$, vs. velocity. The temperatures which were selected as free parameters are indicated in the figure, the pressure is 1 atmosphere and the laser wavelength is $\lambda = 193.1272$ nm.

Fig.14. Temperature and density corrected FD, $N_D = N_D/N_c$, vs. velocity. The pressures which were selected as free parameters are indicated in the figure, the temperature is 100K and the laser wavelength is $\lambda = 193.1272$ nm.

Fig.15. Velocity measurement uncertainty $\Delta v/v$ vs. temperature for the laser tuned to the $v'(0)-v'(13)$ R13 transition. The solid line presents the total uncertainty which is composed of the uncertainty in the temperature and density measurements and $\Delta N_D/N_D = 1\%$. The ($\cdot-\cdot\cdot$) presents the uncertainty when using the temperature and density corrections. The dotted line presents the uncertainty when the only error is $\Delta N_D/N_D = 1\%$. The dashed line presents the measurement uncertainty when the only error is $N_D = \sqrt{N_D}$.

1. INTRODUCTION

The development and the design of advanced hypersonic vehicles such as the National Aerospace Plane (NASP) or the Space Shuttle will strongly depend on computer simulation mainly because some of the flight conditions experienced by these vehicles will be difficult or prohibitively expensive to create in ground facilities. Computer simulation will be used to reduce the need for expensive test time or will replace those experimental tests which can not be performed. However, computer simulations require validation before their results can be accepted. These validation tests, which must be performed in hypersonic and turbulent air flows, require the simultaneous measurement of air temperature, density and velocity at a high temporal and spatial resolution which will allow to resolve turbulence structures. The accuracy of the diagnostic system should be in the neighborhood of 1% and the system must respond well both to cold-air flows (>100 K) in the free stream and hot-air flows (>1000 K) experienced at the stagnation point. Furthermore, elimination of air seeding requirements will simplify the measurement and will allow its application in any facility.

We have been engaged for more than two year (under NASA contract # NAS2-12410) in the development of a technique for the measurement of air temperature and density using an Argon-Fluoride (ArF) laser. The technique applies Laser-Induced Fluorescence (LIF) in molecular oxygen for the temperature measurement, and Raman scattering from nitrogen and oxygen for the density measurement. Our efforts have already identified the measurement potential and restrictions [1,2] of the proposed technique and are now directed toward the demonstration of this approach and towards the engineering of the working device.

In addition, we have started under an SBIR contract from DARPA [3] and under the present funding to investigate the possibility of applying an ArF laser for velocity measurements of unseeded, hypersonic, cold-air flows. We expect that this extension of our work will lead to the development of an integrated system which will be capable of measuring simultaneously the temperature, density and velocity of unseeded-air flows.

We proposed to study under the present contract two velocity measurement techniques which will both rely for the measurement on an ArF laser. In the first approach the air velocity is to be measured by using an intense ArF laser pulse which dissociates atmospheric CO_2 into CO and atomic carbon. The atomic carbon is a strong absorber at 193.1nm and a strong radiator but it is short lived radical in most flow situations. The CO molecule on the other hand is chemically stable and may reside indefinitely in the air flow. Therefore, we proposed to use the CO molecule as a tracer in a modified "Time-of-Flight" velocimetry technique. We have already identified the optimal measurement approach [3]. Here we investigated the effects of air temperature and density and the irregularities in the distribution of the energy across the laser beam on the accuracy of the velocity measurement. We have also conducted a preliminary experiment where the sensitivity of the technique to supersonic air flows was tested. The results of these studies are reported in section 2.

In the second approach the air velocity is to be measured by the Doppler shift experienced by the moving absorbing molecules. In this technique the spectral shift between the absorption wavelength of molecules at rest and the absorption wavelength of the moving molecule is measured. We have already estimated the potential and accuracy of this technique [3]. Here, we evaluated the potential of this technique and estimated the effects of air temperature and density on the measurement accuracy. Since the signal varies linearly with laser intensity we did not have to investigate the effect of the energy distribution across the beam. We described these results in section 3.

2

2. FLOW TAGGING WITH CARBON ATOMS

The CO_2 molecules which are present in air (at .03% mole fraction) can be dissociated by the ArF laser into CO and O (see figure 1). At 193 nm this is a single-photon spin-forbidden dissociation into ground-state products [4]. The variation of the absorption-coefficient with wavelength in the UV was measured [4] in a cell containing 700 torr of CO_2 at 300 K. It was shown to be a monotonously decreasing curve with an absorption coefficient at 193 nm of $\alpha_1 = 0.1$ m^{-1}. The line-width of the ArF laser is narrow relative to the spectral variations of this curve and therefore this absorption coefficient is approximately constant throughout the tuning range of the laser. Although this is a weak absorption, a large fraction of molecules may be dissociated when irradiated by an intense ArF laser. The number density of CO_2 molecules at 700 torr and 300 K is $N_{co2} = 2.2 \cdot 10^{25}$ #/m^3. The absorption cross-section is therefore:

$$\alpha_1/N_{co2} = 0.1/2.2 \cdot 10^{25} = 4.55 \cdot 10^{-27} \text{ m}^2 \tag{1}$$

The product molecules are further dissociated, via a two-photon process, into atomic carbon which is left in the 2^1D state [5]. The two-photon absorption coefficient for this process is [6] $\alpha_2 = 5 \cdot 10^{-11}$ m^4/watt. Finally, the carbon atom is resonant with the laser radiation at 193.1 nm (see figure 1) and may therefore be excited into the 3^1P state from which it radiates at 247.8 nm while decaying into the 2^1S state [5]. The Einstein A coefficient for the transition from 3^1P to 2^1D is [7] $A_{DP} = 2.4 \cdot 10^8$ sec^{-1} and for the transition from 3^1P to 2^1S is [7] $A_{PS} = 3.4 \cdot 10^7$ sec^{-1}. While the interaction of CO with the ArF laser was observed by Bokor, et al.[5] the overall process which starts with atmospheric CO_2 was observed recently by the present principal investigator [1].

MULTI-PHOTON INTERACTION OF ArF LASER WITH CO_2

$$CO_2 + h\nu \longrightarrow CO + O$$
$$CO + 2h\nu \longrightarrow C(2^1D) + O$$
$$C(2^1D) + h\nu \longrightarrow C(3^1P)$$
$$C(3^1P) \longrightarrow C(2^1P) + h\nu(267.8 \text{ nm})$$
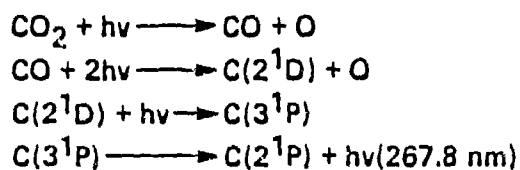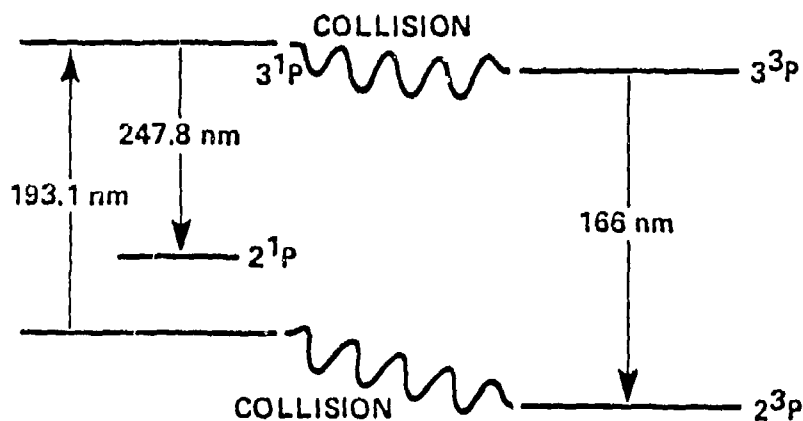
ENERGY LEVEL DIAGRAMS FOR ATOMIC CARBON

Figure 1: The photo-dissociation of CO_2 and CO and the energy level diagram for the LIF in atom carbon.

4

In a previous work [3] we determined which of the intermediate products of this process is long-lived and therefore the most likely to follow the flow and be detected at a latter time by delayed probing. It was demonstrated that carbon atoms in the $C(2^1D)$ state are short-lived. They recombine with N_2 and O_2 to form new molecular species. Therefore, the time dependent concentration of these laser generated atoms follows very closely the temporal variations of the laser pulse itself. Unless the flow is extremely fast, these atoms will combine with other air constituents before moving out of the laser beam. The number density of the CO molecules was shown to remain constant long after the laser intensity has diminished. Thus, only the CO molecules, which are stable, may be generated by the laser pulse at one location and be probed downstream to determine their new location and hence their speed. In contrast, the carbon atoms which are eliminated from the flow by several high-rate mechanisms may not serve as a flow-tagging species.

2.1   SINGLE PULSE CARBON VELOCIMETRY

Although the generation of the CO molecule by the ArF laser is a straightforward process, the probing of this molecule is complex. The wavelength of the dipole-allowed transition between the ground-state and the nearest electronic state in CO is in the vacuum UV [8]. Thus, single-photon excitation of the molecule cannot be obtained with conventional sources. Instead, a two-photon pumping scheme must be employed. One such scheme was already demonstrated for trace species diagnostics in flames [9]. In this technique, two photons at 230.1 nm are used to excite the CO molecule from the $X^1\Sigma^+(v''=0)$ to the $B^1\Sigma^+(v'=0)$ state. The resulting fluorescence is in the $B^1\Sigma^+$ to $A^1\Pi$ Angstrom system within the spectral range of 451 nm to 725 nm. The laser radiation for this excitation is derived from a doubled Nd:YAG laser which pumps a pulsed dye laser. The output of

5

the dye laser is doubled and mixed with the residual radiation of the Nd:YAG laser at 1064 nm.

An experiment was performed on a CO-air diffusion flame [9]. The lowest mole-fraction measured in that flame was 14% or $5.9 \cdot 10^{23} m^{-3}$ at 1900 K. Based on this result, the detection limit was estimated to be $4.0 \cdot 10^{20} m^{-3}$ at 300 K [9]. This exceeds the calculated concentration of CO molecules produced in a single pulse [3]. Thus, it may be concluded that the present two-photon LIF technology does not offer the sufficient sensitivity required for the detection of CO traces generated from atmospheric CO_2 within a single-pulse of the ArF laser.

As an alternative to the conventional Time-of-Flight technique we proposed [3] to investigate a new approach in which the tracer-generation and tracer-probing pulses converge into a single pulse. In this approach the tracer CO molecules are generated within the high intensity ArF laser beam. The intense radiation may further dissociate the molecule, in a two-photon process, into a $C(2^1D)$ atom and an $O(^3P)$ atom. The ArF laser at $\lambda = 193.1nm$ is resonant with the transition from the $C(2^1D)$ level to the $C(3^1P)$ level. Therefore, excitation of the carbon atoms is extremely efficient and may take place, due to power-broadening, at wavelengths which are slightly off resonance. In practice most of the energy of a broad-band ArF laser is coupled into this transition [5]. The excited atoms finally radiate at 247.8. Although this laser-induced fluorescence is a four-photon process it benefits from the high transition-probability in the carbon atom. Therefore, at tight focusing conditions, the intensity of the radiation at $\lambda = 247.8$ nm is comparable to other radiative processes induced in air by the ArF laser [1].

The intensity of the fluorescent radiation in this four-photon process is proportional to the density of CO molecules. Two competing mechanisms determine the density of these molecules along the laser beam path: The dominant mechanism is the generation of CO molecules by the dissociation of CO_2. However, High speed air flow across the laser beam

removes some of the generated CO molecules. This removal process which competes with the generation process reduces the carbon-fluorescence intensity. Therefore, the reduced fluorescence intensity may serve for the measurement of the air-flow velocity across the beam.

In our earlier work [3] we derived the rate equations which describe the time-dependent concentration of the CO molecules, the concentration of the radiating carbon atoms and the concentration of the carbon atoms which were trapped in a metastable state or were chemically removed from the flow. Normally, rate equations include only time-dependence. They do not include any spatial dependence nor can they account for the drift of species by the moving air. To include the effect of gas flow across the laser beam the time-derivative operator d/dt must be replaced with the material-derivative operator D/Dt [10]:

$$D/Dt = \partial/\partial t + U \cdot \nabla \qquad (2)$$

where U is the flow-velocity vector and ∇ is the gradient operator. The velocimetry technique described here is sensitive mostly to the flow rate across the beam. It is insensitive to drift along the laser beam. To increase sensitivity, the narrow dimension of the typically rectangular ArF beam, will be aligned with the cross-flow (see figure 2). Therefore, the material derivative operator may be reduced to a one dimensional operator:

$$D/Dt = \partial/\partial t + u \cdot \partial/\partial \qquad (3)$$

where u is the cross-flow velocity.

By introducing the material-derivative operator into the rate equations they become spatially dependent. Thus, the initial conditions and all the variables, such as the laser-beam intensity, must also be given their spatial distribution. Since the initial density of CO_2 is homogeneous, the laser-beam intensity is the only forcing term with a non-uniform spatial distribution. A typical ArF laser beam is emitted with a cross-section of 1x2.5cm and has an approximately uniform intensity distribution across both dimensions. However,

7
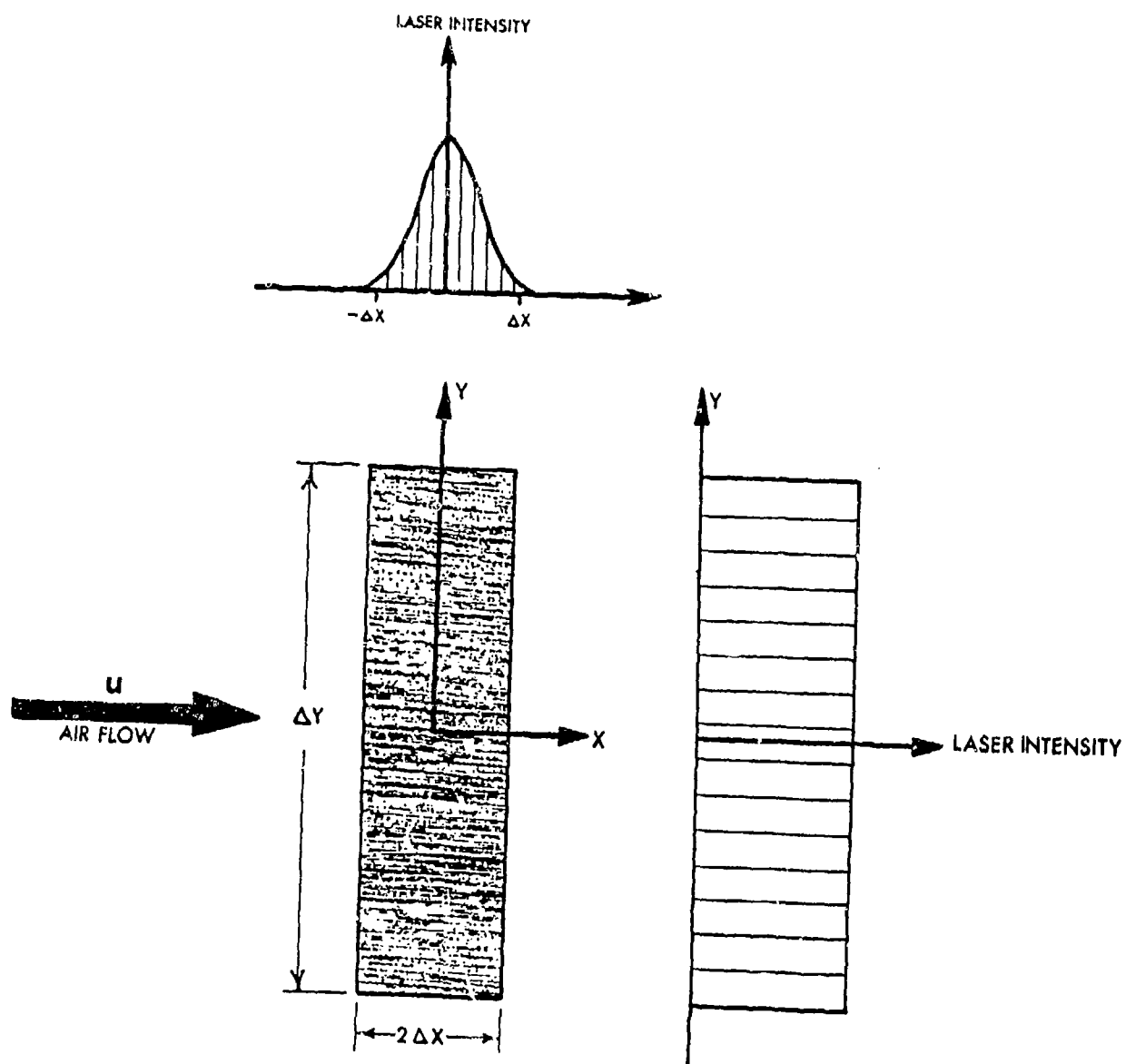
Figure 2: Schematic of the energy distribution across the laser beam.

8

when a plane-wave radiation with an energy E_o and with a uniform intensity distribution is focused, the intensity distribution at the focal plane is [11]:

$$I = \frac{E_o \Delta X \Delta Y}{\tau \cdot \lambda^2 f^2} \, \text{sinc}^2 \left(\frac{x\Delta \bar{X}}{\lambda f}\right) \text{sinc}^2 \left(\frac{y\Delta Y}{\lambda f}\right) \tag{4}$$

where x an y are the coordinates in the focal plane, $\Delta \bar{X}$ and ΔY are the unfocussed beam width and height respectively, f is the focusing lens focal length, τ is the pulse duration and:

$$\text{sinc}(x) = \frac{\sin \pi x}{\pi x} \tag{5}$$

In most applications to be described, the x dimension will be much narrower than the y dimension. Hence, the intensity distribution may be simplified by describing the intensity distribution in the y direction as being uniform and assigning for the intensity distribution in the x direction the following equation:

$$I = \frac{E_o \Delta X}{\tau \cdot \Delta Y \lambda f} \, \text{sinc}^2 \frac{x\Delta \bar{X}}{\lambda f} \tag{6}$$

To further simplify the analysis, the distribution in the x direction may be replaced by a Gaussian intensity-distribution. After normalization, the intensity distribution is:

$$I = \sqrt{\frac{2}{\pi}} \frac{I_o}{\Delta X \Delta Y} \, \exp\left(\frac{-2x^2}{\Delta X^2}\right) \tag{7}$$

where ΔX is the coordinate in the x direction at which the intensity falls to $1/e^2$ of its centerline value and I_o is the intensity at the beam centerline. Usually $2\Delta X$ is considered as the beam width. Introducing also the time dependence, which was assumed to be represented by an exponential decay [3], we obtain:

$$I = \sqrt{\frac{2}{\pi}} \frac{E_o}{\Delta X \cdot \Delta Y \cdot \tau} \exp\left(\frac{-2x^2}{\Delta X^2}\right) \exp\left(\frac{-t}{\tau}\right) \tag{8}$$

9

Here E_0 is the pulse energy and r is the time at which the intensity decays to $1/e$ of its initial value. Usually, r is considered as the pulse duration. The rate equations [3], together with the material-derivative operator (equation (3) and equation (8)) describe the time-dependent spatial-distribution of the dissociation products and of the flux of fluorescence photons at 247.8 nm produced by a focused ArF laser beam which is probing the air-flow.

2.2   RESULTS

2.2.1   FLUCTUATIONS IN THE LASER INTENSITY PROFILE

Equation (8) presents a realistic distribution of the energy across the laser beam profile. This equation is sufficient for accurately predicting the total radiation emitted in linear fluorescence processes. However, in interactions which depend non-linearly on the laser intensity, even slight variations in the intensity distribution, may create large fluctuations in the induced fluorescence energy. Like most gas lasers the intensity profile of the ArF laser may present some pulse to pulse fluctuations which are induced by irregularities in the excitation discharge. To estimate the extent of this effect we introduced two alternative intensity distribution functions and calculated the total carbon fluorescence which will be induced by laser beams with such distributions while all other parameters remain unchanged.

To simulate the effect of 'hot spots' we presented the laser beam as a superposition of two Gaussian distributions offset from the beam centerline. The new distribution function was normalized such that the total energy, E_0, was equal to the total energy delivered by the single Gaussian distribution beam. The new distribution which presents two intensity spikes is:

$$I = \sqrt{\frac{2}{\pi}}\, \frac{E_o}{\Delta X 2\Delta Y \cdot \tau}\, \exp[-2(\frac{x\pm x_0}{\Delta X^2})^2]\ \exp(\frac{-t}{\tau}) \qquad (9)$$

where x_0 is the displacement of the Gaussian distribution from the beam centerline. In addition, we also simulated a homogeneous energy distribution in which all the energy is uniformly distributed within a spot of dimensions of $2\Delta X 2\Delta Y$. The distribution function for this configuration is:

$$I = \frac{E_o}{2\Delta X \cdot \Delta Y \tau}\, \exp(\frac{-t}{\tau}) \qquad (10)$$

Also here the total energy under the distribution curve is E_o.

A numerical code was developed [3] and used to solve the time dependent and spatially varying rate equations. In this code, each solution step included: (a) an explicit forward-difference solution [12] of one half-step in the convection term while the time is held constant, followed by (b) a predictor-corrector solution of one time-step while the the convection term is frozen, followed by (c) the remaining half step in the explicit-forward-difference convection term.

The stability of this algorithm is limited by the explicit-forward-difference steps, with a stability criterion of [12]:

$$u \cdot \delta t / \delta x << 1 \qquad (10)$$

where δx and δt are the sizes of the spatial and time steps in the algorithm.

The integration limits in the calculation were $|x| < 4\Delta X$ and $t < 4\tau$. Beyond these limits, the intensity of the laser, for all distribution functions, was less then 1.8% of its maximum. The number of steps in the x direction was set to 200 while the number of time step was selected individually for each velocity using equation (10). Owing to the uniform inten-

sity distribution in the y direction, the beam height, ΔY, could be selected arbitrarily. It was chosen, however, such that $E_0 = 100mJ$ for a prescribed intensity.

To illustrate the effect of an air-flow across the laser beam on the density of the various carbon species and on the total fluorescence intensity at 247.8 nm we solved the algorithm for a case in which $E_0 = 100$ mJ, $\tau = 20$nsec, $\Delta X = 10\mu m$, $\Delta Y = .399$ mm, and for velocities ranging from $u = 0$ to 2500 m/sec. This focusing configuration corresponds approximately to the highest photon-flux which may be obtained without inducing air breakdown [1,2]. The peak intensity for the single Gaussian distribution was $I = 1 \cdot 10^{15}$ watts/m^2. It was assumed in the calculation that the narrow dimension, i.e. ΔX, is parallel to the main flow-velocity component.

The photon-flux emitted by the excited C atoms when $v = 0$ m/sec and when the intensity distribution is described by a single Gaussian is $1.435 \cdot 10^{13}$ photons/m^2. We assume that the radiation is collected with a 1mm resolution. We further assume that the collection of the light is accomplished by an f/2 lens, that the fluorescence is separated from the background radiation by a band-pass filter with an efficiency of $\eta = 0.5$ and that the photo-detector quantum efficiency is $\eta_d = 0.15$. With these, the number of photo-electrons observed at $\lambda = 247.8$nm by focusing 100mJ of radiation at 193.1nm into atmospheric air is $N_{pe} = 16871$ photons. Similarly when $u = 200$ m/sec $N_{pe} = 15490$ photons and when $u = 2400$ m/sec $N_{pe} = 4546$ photons.

Figure 3 describes the number of photo-electrons detected at 247.8 nm vs the flow velocity for the three different intensity distribution functions. For all distributions $\Delta X = 10\mu m$. The solid line describes the total fluorescence observed when the intensity distribution is a single Gaussian, the doted line corresponds to the double Gaussian distribution where $x_0 = 5\mu m$ while the dashed line corresponds to the uniform distribution. To simplify the comparison, all curves were normalized by 16871 photo-electrons which is the count when $u = 0$ and the energy distribution is described by a single Gaussian.

$\tau = 20$ nsec., $E_0 = 100$ mJ, $N_{pe\,(u=0)} = 16871$ count

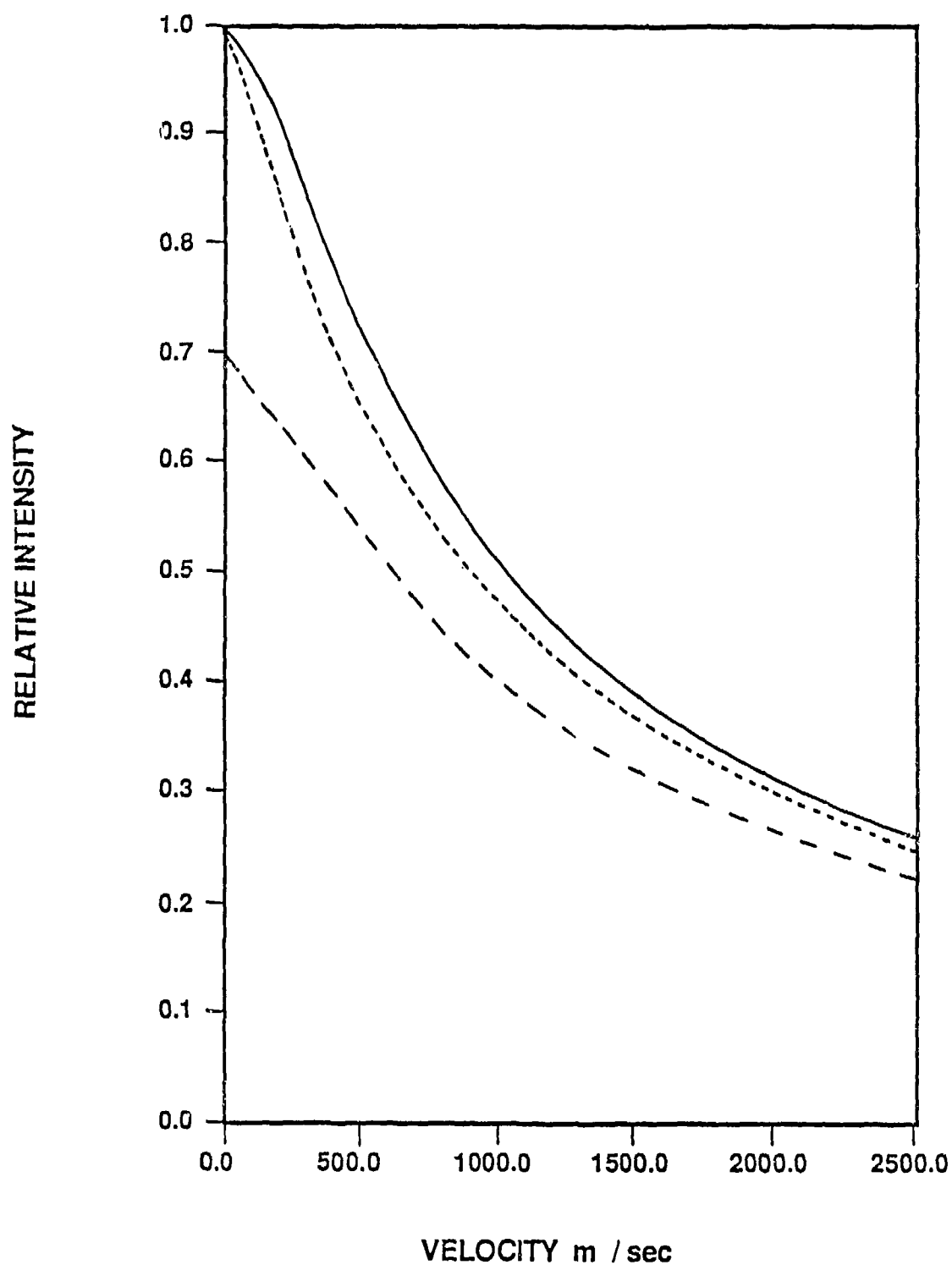Figure 3.   Total fluorescence at 247.8 nm vs the flow velocity for the three different intensity distribution functions. The solid line describes the total fluorescence observed when the intensity distribution is a single Gaussian, the dotted line corresponds to the double Gaussian distribution where $x_0 = 5\mu m$ and the dashed line corresponds to the uniform distribution. For all distributions $\Delta X = 10\mu m$.

It is seen from this figure that when the distribution of the intensity across the laser beam varies, the number of observed photons will vary as well. It is impossible to predict the intensity distribution patterns when the discharge is unstable. Therefore, we assumed that any one of the distributions which are described here may occur at random. In such a case the fluorescence intensity will fluctuate randomly as well. At low velocities the measurement error may be as high as 100%. When the air velocity is 1000 m/sec the number of detected photons induced by the beam with the single Gaussian distribution equals to the number of photons which are induced by the beam with the uniform distribution when the velocity is 604 m/sec and to the number of photons which are induced by the beam with the double Gaussian distribution when the velocity is 875 m/sec. This corresponds to an uncertainty in the velocity measurement which may be as high as 40%. Similar absolute errors will be observed when the air speed is 2500 m/sec. Here however the relative uncertainty is less than 16%.

2.2.2 THE EFFECT OF TEMPERATURE AND DENSITY ON THE MEASUREMENT ACCURACY

Most laser induced fluorescence interactions are temperature dependent. In equilibrium, the population of individual states vary with temperature according to the Boltzmann's distribution. Therefore, when individual states are excited by a narrowband laser the total fluorescence reflects the temperature dependence of the population of the initial state. In addition, at elevated temperatures, dissociation of the ground state and of the excited molecules reduces the density of the interacting molecules and thereby the intensity of the observed fluorescence. Finally, Doppler and pressure broadening are temperature dependent and may affect the coupling between a narrowband laser and the

14

probed molecules. We investigated the effect of temperature on the fluorescence intensity emitted by C atoms following a four-photon dissociation and excitation of CO_2.

The dissociation of CO_2 and CO by the ArF laser is broadband in nature. The interaction does not depend on the excitation of an individual line. Instead it is represented by a transition from the ground state into an upper state continuum. Therefore, the dissociation process which does not depend on the population of an individual level in the ground state is independent of temperature. The interaction with the atomic carbon is line specific. Although this is expected to be an atomic narrowband transition, it appears, due to power broadening, almost as broad as the tuning range of the ArF laser [3]. Therefore, the effects of the Doppler and pressure broadening mechanisms is expected to be negligible. In addition, all carbon atoms here are prepared at the 2^1D state by the dissociation process. Therefore, the population density at this state is determined by the laser parameters and by the concentration of the CO_2 molecules and not by the equilibrium temperature. Furthermore, most of these atoms are consumed by various recombination processes which occur within one collision. As a result, the population of this state cannot be equilibrated and it remains temperature independent.

It is expected that only dissociation of CO_2 or CO which occurs at elevated temperatures can affect the total fluorescence emitted by the C atoms. This effect is likely to be small at room conditions but may become significant in high temperature stagnation points or in reacting flows.

To examine this effect we calculated the chemical equilibrium of dry air using the STANJAN iterative computer program which was developed by W.C.Reynolds from Stanford University.

The program models the gas as a mixture of ideal gases and possibly condensed phases in the form of liquid droplets or solid particulates. The thermodynamical data base is taken from the JANAF tables and is structured accordingly. The user is expected to iden-

15

tify the species of the mixture, the relative concentration of the atomic components, and two independent thermodynamic properties of the state at which the equilibrium is sought (e.g. temperature and pressure). The calculation of the equilibrium is based on the method of element potentials in which exact equations for the gas-phase mole fractions are derived in terms of Lagrange multipliers and the total number of moles is adjusted to meet the various atomic concentrations and to render the sum of the mole fractions to unity. Thus, in mixtures which involve N species but only M atoms (where $N>>M$), the program requires the adjustment of only $M+1$ parameters. This is in contrast to most equilibrium analysis techniques where all the unknown mole fractions need to be adjusted.

We used a modified IBM PC version of this program. We applied it for the equilibrium analysis of air which included the following constituents with their initial molar fraction: 0.7809 N_2, 0.2095 O_2, 0.0093 Ar, and $0.0003 CO_2$. The program was tested by comparing the calculated equilibrium mixture of air at 1 atm and at temperatures of 1500 K and 2500 K with the equilibrium mixture obtained by using the CEC72 equilibrium program which was developed by Svehla and McBride from NASA Lewis. The results of of the CEC72 program agreed with the results of the STANJAN program within 1%. This confirmed the accuracy of the STANJAN program.

The variation of the molar fraction of CO with temperature is presented in figure 4 while the temperature dependence of CO_2 is presented in figure 5. The pressure for these calculations was kept at 1 atmosphere while the temperature was varied between 1000 - 3000 K. The relative concentration of CO is below 10^{-6} throughout the whole temperature range of interest. This concentration is small relative to the concentration of CO following laser induced CO_2 dissociation. The molar fraction of CO_2 is shown in figure 5 to be independent of temperature when the air temperature is below 2000 K. At higher temperatures, dissociation takes place, the concentration of CO_2 decreases while the concentration of C increases. Therefore, below 2000 K, when the CO_2 concentration is temperature
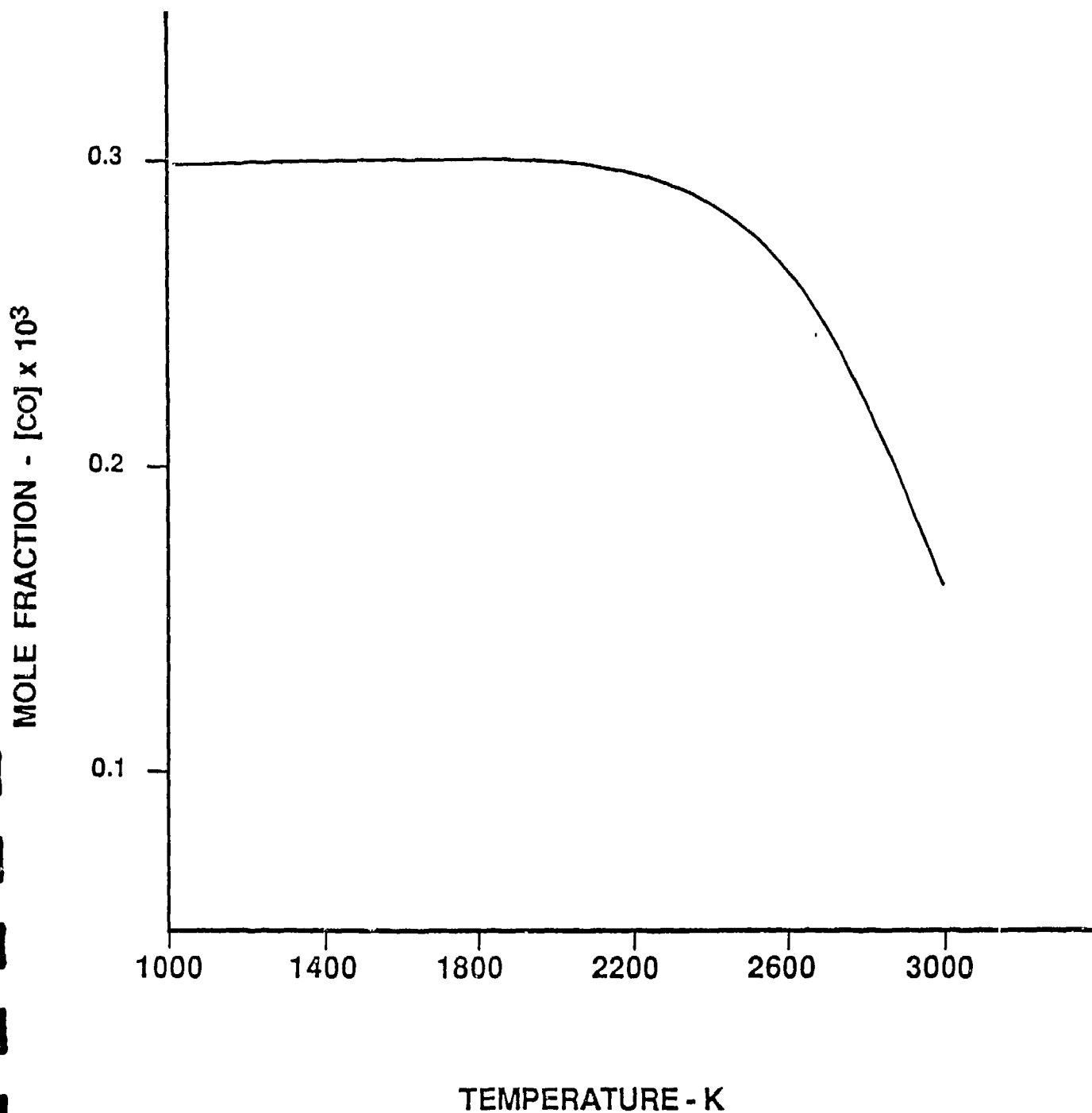
Figure 4:   The variation with temperature of the molar fraction of CO in air in terms of $\log_{10} (10^{13} \cdot [CO])$.
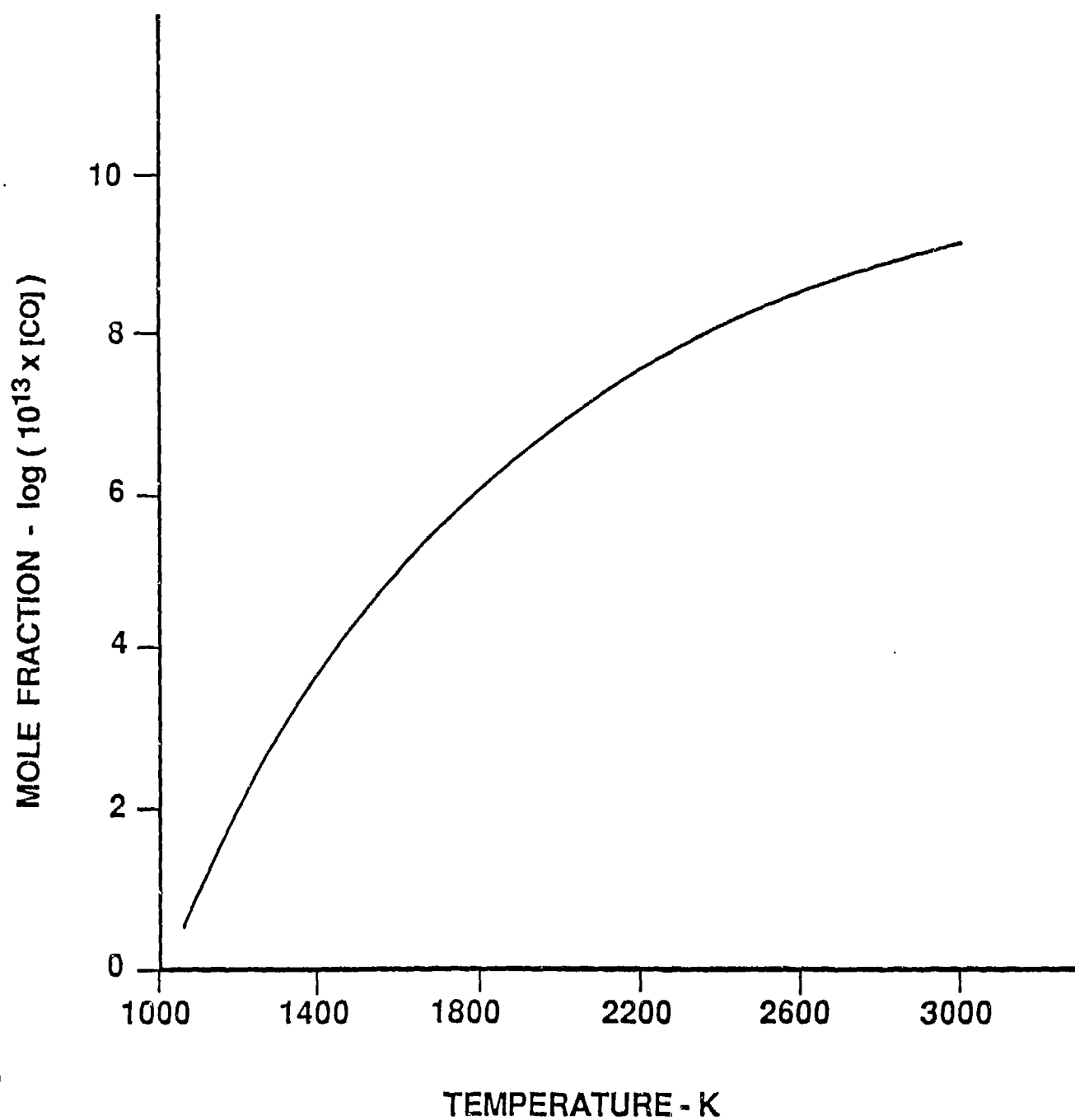
Figure 5: The variation with temperature of the molar fraction of CO_2 in air in terms of $10^3 \cdot [CO_2]$.

18

independent, the fluorescence intensity emitted by C atoms at 247.8 nm is expected to be temperature independent. Therefore, a single measurement of the total fluorescence at 247.8 nm and of the gas density will yield the flow velocity across the laser beam. Note that both the CO_2 and CO concentrations vary linearly with the initial air density. Therefore, these results are expected to be valid also at other densities. We repeated our calculations for P = 0.01 atm and for P = 10 atm and found that also at these pressures the CO_2 concentration was independent of temperatures when the air temperature is below 2000K.

2.2.3 EXPERIMENTAL TESTING OF THE FEASIBILITY OF THE TECHNIQUE

The single pulse carbon velocimetry is expected to be sensitive to the velocity of high speed flows. We tested the feasibility of this technique by comparing the total fluorescence emitted by the dissociation products of atmospheric CO_2 in stationary air with the total fluorescence emitted in supersonic jets.

The experimental setup included a broadband ArF laser which emits 250 mJ/pulse at $\lambda = 193$ nm at a rate of 10Hz. The beam was focused by a lens with a focal length of 150 mm. The spot size was estimated, using a Polaroid film burning, to be less than 100 μm. This was the tightest focusing, using this amount of energy, which could be obtained without inducing an air breakdown. The induced fluorescence was collected by an f/2 lens and was imaged on the slits of a Jarrel-Ash 0.5 m monochromator which was equipped with a 1180 grooves/mm grating blazed at 5000 A and a solar blind photomultiplier tube (PMT). The output of the PMT was monitored by a 100 MHz oscilloscope. The monochromator slits were set at 250 μm. This was the largest slit width which still allowed to resolve the 247.8 nm carbon line from the adjacent oxygen fluorescence line.

To create a supersonic jet we designed a 1/8" orifice which could be mounted on the end of a tube which was connected to a high pressure air cylinder. The expansion ratio was

designed such that for stagnation conditions of 150 psi and 25 C and for an isentropic fully expended flow the exit Mach number was $M=2.2$. To assure that the jet is correctly aligned both with the tightly focused beam and with the collection cone we used initially a helium flow. When the jet was aligned correctly the signal both due to the carbon line and due to the oxygen fluorescence diminished. When the supply line was reconnected to the air supply the signal recovered.

We performed two measurements of the fluorescence intensity: a measurement with the laser beam propagating through the stationary room air and a measurement with the beam propagating through the supersonic jet. The intensity measurements in both experiments were approximately identical although the high speed flow across the beam was expected to reduce the fluorescence intensity. Changing the stagnation pressure and hence the total density also did not have any noticeable effect on the observed fluorescence.

In a subsequent work under our NASA contract we studied some of the properties of the non-linear process in CO_2. It was concluded that when the laser fluence exceeds 1.5 J/cm^2, ionization and quenching effects interfere with the dissociation and excitation processes. As a result, the otherwise third order process may appear as almost independent of laser intensity or gas density. The maximum fluence in the present experiments was 2000 J/cm^2. This fluence exceeds the minimum fluence of $1.5/J/cm^2$ at which the non-linear process follows the predictable third-order behavior. On the other hand, the minimum fluence which is required to obtain an accuracy of at least 5% is 66 J/cm^2 [3]. The difference between the minimum fluence required for high accuracy and the maximum fluence at which ionization and quenching effects are negligible is too large and can not be reconciled.

It is advantageous to use high fluence for these measurements. However, the interpretation of the fluorescence measurements for single pulse carbon velocimetry must include also an analysis of the interfering ionization and quenching effects. This analysis is

20

more complex than the interpretation of the results of the third order process. In addition, the normalization of signals can not rely on a simple calibration cell. Therefore, we believe that the ionization and quenching effects associated with the required high fluence make the single pulse carbon velocimetry too complex for most wind tunnel applications.

3.   DOPPLER VELOCIMETRY

An alternative to the CO velocimetry is a velocity measurement technique which relies on the Doppler shift experienced by molecules moving in the gas stream. This technique was originally proposed and demonstrated by one of the co-workers of this project (Zimmermann [13]). In this technique, the molecules are excited by a tunable dye-laser and their excitation is marked by the fluorescence decay from the excited state. The difference between the frequency needed to excite stationary molecules and the frequency at which the moving molecules are excited is the Doppler shift. This shift is proportional to the gas velocity.

Several schemes for the measurement of the Doppler shift have been proposed. Zimmermann used successive counter-propagating beams to measure the frequency difference between the up-shifted and down-shifted frequencies of the D lines of Na atoms seeded into a He flow [13].

She [14], Exton [15] and others proposed to replace the LIF technique, which was used to measure the Doppler-shift, with a coherent Raman process such as the Inverse-Raman-Spectroscopy (IRS) or CARS. Both these coherent Raman schemes require a fixed frequency laser and a synchronously pumped narrow-band tunable laser which is tuned to excite the Raman process. When the two laser beams which are required for the excitation of the Raman process are counter propagating, the Doppler shift sensed by the molecules and the measurement sensitivity are doubled. Co-propagating beams are usually used in stimulated Raman spectroscopy to suppress the Doppler shifts. Both the LIF and the Raman Doppler techniques are slow. The time required to tune the probe laser until the Doppler shift is measured may last up to few minutes per point and therefore is suitable only for time-averaged measurements [13].

22

Hiller et al.[16] proposed a method which removes this difficulty. In their approach, two counter-propagating laser beams are tuned to the high frequency wing of the absorption line of I_2 molecules seeded in a N_2 subsonic flow. In the absence of flow, both beams encounter the same absorption cross-section of the I_2 molecules and induce the same fluorescence intensity. However, when the absorbing molecules move along the laser beams together with the gas flow, the absorbed radiation is Doppler shifted: the frequency of the radiation of the beam which propagates opposite to the flow is Doppler up-shifted and is therefore further away from the absorption line-center. Therefore, fluorescence intensity induced in molecules which move opposite to the beam decreases. The other laser beam - which propagates in the direction of the N_2 flow - is experienced by the moving molecules as Doppler down-shifted. Therefore, the fluorescence induced by this beam will be more intense. The difference in intensities between these two LIF processes has been shown by Hassa et al. [17] to relate to the flow velocity.

To further simplify this Fluorescence Difference (FD) velocimetry technique and to eliminate the need for seeding we proposed [3] to use an absorption line in the Schumann-Runge band of O_2 for monitoring Doppler shifts experienced by these molecules in air flows. This technique benefits from the coincidence between the frequency of the ArF laser and the absorption frequency of O_2 in the Schumann-Runge band. In this transition the O_2 molecule is excited from the $X^3\Sigma_g^-$ electronic ground state to the $B^3\Sigma_u^-$ electronic excited state [18]. This approach is compatible with our ongoing effort of developing laser techniques for the measurement of air temperature and density in hypersonic wind tunnel flows.

The measurement uncertainty of all Doppler techniques is determined primarily by the spectral line width of the laser and by the width of the transition line of the probed molecule. The reported line-width of the only commercially available tunable ArF laser is $\Delta\nu_L = 9$ GHz [19]. The natural line-width $\Delta\nu_u$ of the v"(0) to v'(4) transition of O_2,

which may be excited by the ArF laser, is 125.4 GHz [20]. This extremely large width is due to the predissociation of the upper state. For comparison, the Doppler shift $\Delta\nu_D$ of the moving flow is [21]:

$$\Delta\nu_D = \nu \cdot u/c = u/\lambda \qquad (11)$$

For a flow of $u = 1000$ m/sec and for a wavelength of $\lambda = 193.3$ nm, the Doppler shift is 5.17 GHz. This shift is small relative to the v"(0) to v'(4) transition line-width and is comparable to the laser line-width. Although the application of an ArF laser beam for the measurement of the Doppler shift experienced by the v"(0) to v'(4) transition of O_2 may yield a qualitative velocity measurement it is unlikely to result in an accurate quantitative measurement. The accuracy of the measurement may be enhanced by selecting a laser wavelength which is resonant with an O_2 transition which presents a narrower line-width. The predissociation life-time of the v'(13) K = 13 level in the $B^3\Sigma_u$ electronic state corresponds to a natural line-width of 4.58GHz [20]. Transitions from the ground state to this state result in a line which is among the narrowest in this manifold of vibrational states and therefore is the most suitable for the Doppler velocimetry technique. This line is resonant with the wavelength of the ArF laser which was Raman shifted with a H_2 Raman cell [22]. This device, which is available commercially, uses high pressure H_2 as the Raman gain medium to shift the wavelength of the beam by 4155 cm^{-1}. If the ArF laser beam is tuned to 193.138 nm the wavelength of the Raman shifted beam will be $\lambda = 178.790$ nm which is resonant with the v"(0) to v'(13) R13 transition.

In a previous work [3], we calculated analytically the measurement uncertainty which is associated with this velocimetry technique. The calculation assumed interaction with only one rotational transition in the v'(0) to v'(13) band. However, the Raman shifted laser beam is also resonant with the v"(0) to v' = 14,15,16 and 17 transitions. Some of these

24

transitions overlap the v"(0) to v'(13) band. Therefore, an accurate prediction of the temperature dependence of this measurement requires the inclusion of all the transitions which are resonant with the laser. We have modified a model which was developed by us under a separate contract [2]. The modified model describes the LIF process in molecular oxygen excited by a Raman shifted beam. The model calculates the intensity of the total fluorescence emitted by an air stream moving along and opposite to a Raman shifted ArF laser beam. Both the air velocity, temperature and density can be included as parameters. In the following sections we describe the model and the results of our calculations.

3.1 THE MODEL OF LIF IN OXYGEN

A computer model which describes the absorption of an ArF laser beam by air and the subsequent induced fluorescence has been developed. The code predicts the effects of absorption by room air of a Raman shifted ArF laser beam with a prescribed initial spectral distribution as it propagates from the laser to the sample volume. The attenuation at each wavelength in the laser bandwidth is evaluated by adding the contributions of all participating transitions that originate from the ground electronic state. The total fluorescence energy which is emitted by the gas in the observed sample volume is then calculated using the spectral distribution of the incident beam at the sampling point.

3.1.1 The Spectroscopic Features of LIF in Oxygen

The calculation of absorption includes all significant rotational transitions which fall within the spectral tuning range of the ArF laser, including the following vibrational bands: from v"(0) to v'(13) v'(14), v'(15), v'(16), and v'(17). No other transitions from v"(0), v"(1) and v"(2) were found to be resonant with the Raman shifted ArF laser throughout its tuning range. The term values of the ro-vibronic levels in the $B^3\Sigma_u^-$ upper electronic state were calculated using the equations and parameters of Cheung et al [23]

which include the fine-splitting of the rotational states. Those upper-state term values together with the term values of the v"(0) and v"(1) levels of the $X^3\Sigma_g^-$ lower electronic state which are given by Veseth and Lofthus [24] reproduce the measured transition frequencies [25] for all tra...sitions originating from the v"(0) and v"(1) state. For transitions from the v"(2) which were not given by Ref. 24, the expressions of Endo and Mizushima [26] for the dependence of the parameters on vibrational quantum number were used. However, their constants were adjusted to reproduce the parameters of the v"(0) and v"(1) states reported by Ref. 24. Thus, for the rotational term values of all the vibrational states in the $X^3\Sigma_g^-$ electronic state, the following expressions were used:

$$B_v = 1.445584 - 0.015778(v+0.5)$$

$$D_v = 4.8425 \times 10^{-6} + 3.3 \times 10^{-8}(v+0.5)$$

$$\lambda = 1.9855 + 7 \times 10^{-4}(v+0.5) \tag{12}$$

$$\gamma = -8.525 \times 10^{-3} - 7 \times 10^{-5}(v+0.5)$$

$$\lambda_D = 1.839 \times 10^{-6}$$

$$\gamma_D = -4.01 \times 10^{-9}$$

where B_v, D_v, λ, γ, λ_D and γ_D are all specified in cm^{-1} and are the same notation which is used in Refs. 23-26. The calculated wavelengths for the transitions from v"(0) and v"(1) matched the measured wavelengths [25] within 0.5 cm^{-1}. No measurements were found to compare with computed results for transitions originating from v"(2) and they are not expected to have the same accuracy as the results for transitions from the lower states. However, since only the transitions from v'(0) were found to be resonant with the Raman shifted beam this will not affect the accuracy of this calculation. Table 1 lists all the transitions and their wavelengths which are resonant with the Raman shifted ArF laser beam.

TABLE 1: <u>WAVELENGTHS FOR THE TRANSITION FROM V"=0 TO</u>
<u>v'=13,14,15,16,&17</u>

<u>THE R BRANCH</u>

<u>V"</u>	<u>V'</u>	<u>K</u>	<u>I</u>	FUNDAMENTAL WAVELENGTH <u>A°</u>	RAMAN SHIFTED <u>W.L.(A°)</u>	<u>FREQUENCY</u>
0	13	11	1	1929.739	1786.497	55975.469
0	13	11	2	1929.681	1786.447	55977.039
0	13	11	3	1929.657	1786.426	55977.680
0	13	13	1	1931.378	1787.901	55931.516
0	13	13	2	1931.314	1787.846	55933.215
0	13	13	3	1931.286	1787.822	55933.980
0	13	15	1	1933.297	1789.545	55880.121
0	13	15	2	1933.228	1789.486	55881.965
0	13	15	3	1933.194	1789.457	55882.863
0	13	17	1	1935.499	1791.432	55821.266
0	13	17	2	1935.425	1791.369	55823.242
0	13	17	3	1935.386	1791.335	55824.277
0	14	19	1	1929.167	1786.006	55990.852
0	14	19	2	1929.051	1785.907	55993.949
0	14	21	1	1932.069	1788.493	55912.988
0	14	21	2	1931.946	1788.388	55916.285
0	14	21	3	1931.879	1788.330	55918.078
0	14	23	1	1935.281	1791.245	55827.082
0	14	23	2	1935.150	1791.133	55830.590
0	14	23	3	1935.075	1791.069	55832.590
0	15	25	1	1932.246	1788.645	55908.234
0	15	25	2	1932.041	1788.469	55913.742
0	15	25	3	1931.926	1788.371	55916.809
0	15	27	1	1936.284	1792.104	55800.328
0	15	27	2	1936.066	1791.917	55806.141
0	15	27	3	1935.939	1791.809	55809.508
0	16	27	1	1931.602	1788.093	55925.508
0	16	27	2	1931.270	1787.809	55934.391
0	16	27	3	1931.088	1787.652	55939.289
0	16	29	1	1936.215	1792.046	55802.152
0	16	29	2	1935.865	1791.746	55811.488
0	16	29	3	1935.665	1791.574	55816.836
0	17	29	1	1933.158	1789.426	55883.828
0	17	29	2	1932.644	1788.986	55897.598
0	17	29	3	1932.354	1788.737	55905.359

27

THE P BRANCH

V"	V'	K	J	FUNDAMENTAL WAVELENGTH A°	RAMAN SHIFTED W.L.(A°)	FREQUENCY
0	13	11	1	1930.625	1787.256	55951.703
0	13	11	2	1930.572	1787.210	55953.125
0	13	11	3	1930.553	1787.194	55953.625
0	13	13	1	1932.416	1788.791	55903.684
0	13	13	2	1932.359	1788.741	55905.230
0	13	13	3	1932.335	1788.722	55905.848
0	13	15	1	1934.488	1790.566	55848.266
0	13	15	2	1934.425	1790.512	55849.949
0	13	15	3	1934.397	1790.488	55850.695
0	13	17	1	1936.842	1792.583	55785.430
0	13	17	2	1936.774	1792.524	55787.250
0	13	17	3	1936.741	1792.496	55788.129
0	14	19	1	1930.516	1787.162	55954.621
0	14	19	2	1930.409	1787.071	55957.500
0	14	19	3	1930.358	1787.027	55958.867
0	14	21	1	1933.551	1789.763	55873.316
0	14	21	2	1933.436	1789.665	55876.301
0	14	21	3	1933.377	1789.614	55877.961
0	14	23	1	1936.894	1792.627	55784.055
0	14	23	2	1936.771	1792.521	55787.336
0	14	23	3	1936.704	1792.464	55789.109
0	15	23	1	1929.976	1786.699	55969.121
0	15	23	2	1929.793	1786.543	55974.016
0	15	23	3	1929.702	1786.465	55976.469
0	15	25	1	1933.782	1789.961	55867.137
0	15	25	2	1933.588	1789.795	55872.328
0	15	25	3	1933.485	1789.707	55875.078
0	16	27	1	1933.008	1789.298	55887.836
0	16	27	2	1932.694	1789.029	55896.246
0	16	27	3	1932.528	1788.887	55900.680
0	17	27	1	1929.505	1786.296	55981.766
0	17	27	2	1929.042	1785.899	55994.203
0	17	29	1	1934.401	1790.492	55850.578
0	17	29	2	1933.912	1790.072	55863.672
0	17	29	3	1933.647	1789.845	55870.754

The dipole matrix-elements which are necessary for the calculation of the transition probabilities were evaluated using an ab-initio method in which the required wave functions for both the $X^3\Sigma_g^-$ and $B^3\Sigma_u^-$ states were obtained from a multi-reference, first-order configuration-interaction calculation with a large Slater basis set [27]. The vibrational wave functions for both states were obtained from a numerical solution of the one-dimensional Schrodinger equation using the RKR potentials tabulated in Ref. 18. The resulting oscillator strengths for the v"(0) to v'(1-12) transitions agreed with low-temperature measurements [28] to within 5%. The transition line-widths were assumed to be dominated by the predissociation rates of the upper states which are given by Ref.20. The collision broadening was included using the following empirical equations derived by Cann et al.[29]:

$$\Delta\nu_p = 0.3P\left(\frac{273.2}{T}\right)^{0.7} \tag{13}$$

where the pressure P is given in atmospheres. For T=300K and P=1atm $\Delta\nu_p$=8.43GHz. The Doppler broadening was assumed to have a Gaussian line shape with a width of [30]:

$$\Delta\nu_D = \frac{2\nu_0}{c\sqrt{\frac{2KT\ln2}{M}}} \tag{14}$$

Where $\nu_0 = 1.68\cdot10^{15}$ Hz is the exciting frequency and $M = 32\cdot1.67\cdot10^{-27}$Kg is the molecular mass of oxygen. At room temperature the Doppler broadening is $\Delta\nu_D$=3.67GHz.

The total line-width of the transition is determined by the accumulation of the Doppler broadening, the pressure broadening and the predissociation line-width. The Doppler broadening is comparable in magnitude to the predissociation line-width. The final line-width however is dominated by the pressure broadening mechanism. Both the pressure

29

and predissociation mechanisms have a Lorentzians line-shape, while the Doppler broadening has a Gaussian line-shape. A convolution between the Lorentzian line-shape and the Gaussian shape must be made to include the Doppler broadening in the calculation. This however requires resort to either polynomial techniques or to a numerical approach for the calculation of the convolution integral. To simplify the calculation we assumed that the shape of the Doppler broadening is also a Lorentzian. This introduces a relatively small error but has the advantage of a much simplified calculation and a broader range of analysis. The combined line-shape is assumed therefore to be a Lorentzian with a line-shape function $g(\nu)$ [21]:

$$g(\nu) = \frac{\Delta\nu_t}{2\pi[(\nu - \nu_0)^2 + (\frac{\Delta\nu_t}{2})^2]} \tag{15}$$

where the total line width $\Delta\nu_t$ is:

$$\Delta\nu_t \approx \Delta\nu_u + \Delta\nu_p + \Delta\nu_D \tag{16}$$

3.1.2   The Fluorescence Signal

The observed fluorescence signal is expected to be proportional to the initial population of the ground-state, N_{10}. Fundamentally, this population is proportional to the gas number density, N_o, and is also a function of the temperature dependent Boltzmann distribution of the molecules among the rotational states. The variation with temperature of the population density, N_J of an individual rotational state may be described by the following equation [31]:

30

$$N_J = \frac{N_{10} \cdot S \, hcB_v}{KT} \; \exp \left(-\frac{E}{KT} \right) \qquad (17)$$

where S is the Honl-London factor h is the Planck's constant, B_v is the rotational constant, E is the energy of the rotational state, $K = 1.38 \cdot 10^{-23}$ J/°K is Boltzmann's constant and $N_o = 0.2P/KT$ is the density of oxygen in air at a pressure P and temperature T.

In most experiments there exists a temperature at which the population density of the ground state reaches a maximum. For illustration, at constant pressure conditions, the temperature for maximum population can be calculated using equation (17) and is:

$$T_{max} = E/2K \qquad (18)$$

It is evident from eqn.17 that the LIF and FD processes depend both on the gas temperature and the density which will need to be measured independently before the velocity can be deduced from the FD signal. We are presently developing an ArF LIF technique for the measurement of the temperature of atmospheric oxygen and a Raman technique for the measurement of the density of air. Both techniques will be used simultaneously with the Doppler velocimetry technique and therefore will provide the additional necessary information.

When an intense laser is used for this measurements, a large fraction of the ground state molecules is excited. Owing to the predissociation effect, only few molecules relax back to their original state. Therefore, the ground-state population during the LIF process may depend also on the laser fluence. While replenishment of ground-state molecules can occur by several mechanisms, one can discard the effects of rotational radiative transitions which are negligible because electric-dipole transitions between rotational states in the O_2

molecule are forbidden and the allowed magnetic-dipole transitions are extremely weak [32]. Thus, only collisional relaxation may redistribute the population among rotational states. However, although the time between collisions at standard temperature and pressure conditions is 0.14 ns, it will be comparable with the 15 ns duration of the laser pulse at low densities. Therefore, at the low gas densities which may occur in hypersonic air flows, the absorbing states which were radiatively depleted will not be equilibrated and the strict linear relation between the total fluorescence and the population density may be violated.

To calculate the population of the absorbing state and the subsequent fluorescence signal, including the effects of predissociation, the absorption and the fluorescence processes are described by the following rate equations:

$$\frac{d(N_1/g_1)}{dt} = \frac{N_2/g_2}{\tau_{21}} - W_{12}(\frac{N_1}{g_1} - \frac{N_2}{g_2}) \tag{19a}$$

$$\frac{d(N_2/g_2)}{dt} = \frac{-N_2/g_2}{\tau_f} - \frac{N_2/g_2}{\tau_D} + W_{12}(\frac{N_1}{g_1} - \frac{N_2}{g_2}) \tag{19b}$$

where $W_{12} = I\sigma_{12}/h\nu$, I is the laser intensity, σ_{12} is the absorption cross-section, $h\nu$ is the photon energy, N_1 and N_2 are the population densities of the lower and upper states respectively, g_1 and g_2 are their degeneracies, τ_{21} is the spontaneous radiative lifetime for the transition from the upper state to the lower state, τ_f is the fluorescence lifetime of the upper state including transitions to all the accessible levels in the ground electronic state, and τ_D is the predissociation time. For all the transitions which can be excited by the ArF laser, τ_D is of the order of 10^{-11} sec while τ_{12} and τ_f are approximately 10^{-5} sec and $W_{12} = 10^7$ sec^{-1}. Because the predissociation rate exceeds all the other rates, we can assume that $N_2 << N_1$ and, therefore, neglect the first terms in eqns.(19a) and (19b). The rate equations can then be decoupled and solved independently to give the result

$$N_1 = N_{10} \exp(-W_{12}t) \tag{20a}$$

and

$$\frac{g_1}{g_2}N_2 = \frac{W_{12}N_{10}\exp(-W_{12}t)}{1/\tau_D - W_{12}} - \frac{W_{12}N_{10}\exp(-t/\tau_D)}{1/\tau_D - W_{12}} \tag{20b}$$

By assuming that $W_{12} << 1/\tau_D$, Eq.(19b) may be reduced to

$$\frac{g_1}{g_2}N_2 \approx \tau_D W_{12} N_{10} \exp(-W_{12}t) \tag{20c}$$

The fluorescence signal may now be defined as the total number of fluorescence photons which are emitted during a laser pulse of duration, τ_p, by the excited molecules enclosed in a volume which is defined by the beam cross-section, A, and the length of the observed beam, L. It is expressed as

$$S_f = A \cdot L \int \frac{N_2}{\tau_f} \, dt$$

$$= A \cdot L \frac{\tau_D}{\tau_f} N_{10}(\frac{g_2}{g_1}) [1-\exp(-W_{12}\tau_p)] \tag{21}$$

where the integration has been simplified by assuming that the spatial and temporal intensity distributions of the laser are uniform. With those assumptions, Eq. (21) may be rewritten in terms of the laser pulse energy, E_p, by describing the average intensity as:

$$I = \frac{E_p}{A\tau_p} \tag{22}$$

33

The fluorescence signal is then:

$$S_f = A \cdot L(\frac{\tau_D}{\tau_f}) \cdot N_{10} \cdot (\frac{g_2}{g_1})[1-\exp(-(\frac{E_p G_{12}}{A \cdot h\nu}))] \tag{23}$$

Note that this expression is a non-linear function of the laser fluence, E_p/A, which, in turn, determines the extent of the depletion of the ground state population by the predissociation process. However, when $W_{12}\tau_p << 1$, or when the rate of collisional redistribution is sufficiently high, the depletion of the ground-state population may be assumed to be negligible. The fluorescence signal then becomes a linear function of the laser intensity according to:

$$S_f(T,\rho) = L\,E_p \frac{\sigma_{12}}{h\nu} \cdot \frac{\tau_D}{\tau_f} \, N_{10}(T,\rho)(\frac{g_2}{g_1}) \tag{24}$$

where the dependence of the fluorescence signal on the temperature and density of the gas volume being probed is indicated.

3.1.3 UNCERTAINTY IN THE VELOCITY MEASUREMENT

A primary goal of this study is to estimate the uncertainty in the velocity measurements. For this analysis, the uncertainty in the velocity measurement is limited by the error in the fluorescence measurement which in turn is assumed to be limited by the photon-statistical noise (the shot-noise). In addition, the fluorescence signal for the temperature measurement and in the simultaneous Raman signal used for the required measurement of density are also assumed to be limited by the shot-noise. These assumptions were verified by us experimentally [2]. The statistical nature of any photoemission or photodetection

34

process results in fluctuations in the total number of photoelectrons, $\bar{N}_e$, which are produced in the photodetector owing to the fluorescence from each laser pulse. These fluctuations appear as noise in the fluorescence signal and are characterized by the expression [33]

$$\Delta \bar{N}_e = \sqrt{N_e} \qquad (25)$$

To estimate the number of photoelectrons, the parameters of the collection optics must be included in the calculation. For example, in a typical experiment the fluorescence from a sample volume of length, L (taken to be 1 mm), is collected by a system of collection optics with a collection efficiency, η_c (equal to .015 for f/2 optics) and detected by a photomultiplier with a quantum efficiency, η_d (typically equal to .15). The detection system may also contain a bandpass filter with a transmission, T_f, which is used to reject background radiation emitted by fluorescing optical components. The result, which is a function of the gas temperature, T, and density, ρ, is then:

$$\bar{N}_e(T,\rho) = S_f(T,\rho)\, \eta_c \, \eta_d \, T_f \, L \qquad (26)$$

where S_f is obtained from Eq.(24). While temperature and density are deduced from a direct fluorescence or Raman intensity measurements, the velocity depends on the difference between two fluorescence measurements, N_D. The relative velocity measurement uncertainty can then be evaluated from

$$\frac{\Delta v}{v} = \frac{2\sqrt{\bar{N}_e} + (\frac{\partial N_D}{\partial T})_{v,\rho}\, \Delta T + (\frac{\partial N_D}{\partial \rho})_{v,T}\Delta\rho}{v(\frac{\partial N_D}{\partial v})_{T,\rho}} \qquad (27)$$

35

where $\Delta\rho$ is the uncertainty in the independent density measurement which is based on the photon-statistical noise associated with the Raman signal and ΔT is the uncertainty in the temperature measurement. The sensitivity of the fluorescence difference signal to velocity is determined by the derivative term in the denominator of Eq.(27). When the photon-statistical noise is high, the uncertainty can be reduced by selecting transitions with high sensitivity, e.g., transitions with a narrow line-width as proposed here.

3.2.   RESULTS

3.2.1   Selection of the Optimal Absorption Line

The excitation spectrum of oxygen is obtained by exciting the gas with a narrow band laser - which is tuned over the absorption bands within its tuning range- while observing the broadband fluorescence signal. The excitation spectrum originating from the absorbing transitions from v"(0) to v'(13), v'(14), v'(15), v'(16) and to v'(17) was calculated by our model while assuming that the ArF laser is continuously tunable between 192.9 nm and 193.7 nm. Consequently, the Raman shifted beam in the calculation was tunable between 178.59 nm and 179.27 nm. The fluorescence signal was assumed to be normalized by the laser pulse energy which, in turn, is measured from a portion of the laser beam going to the sample volume. The beam paths through room air to the sample volume and to the pulse-energy detector had identical lengths. Therefore, the normalization removed the effects both of pulse-to-pulse energy variations and of absorption by room air which varies with laser wavelength.

Figure 6 presents the predicted normalized excitation spectrum of room air which is excited by a Raman shifted ArF laser with a line width of 9GHz and an energy of 1 mJ/pulse. The calculated total fluorescence was multiplied by a transmission function which is centered at 240 nm, has a bandwidth of 10 nm and a peak transmission of 20%.
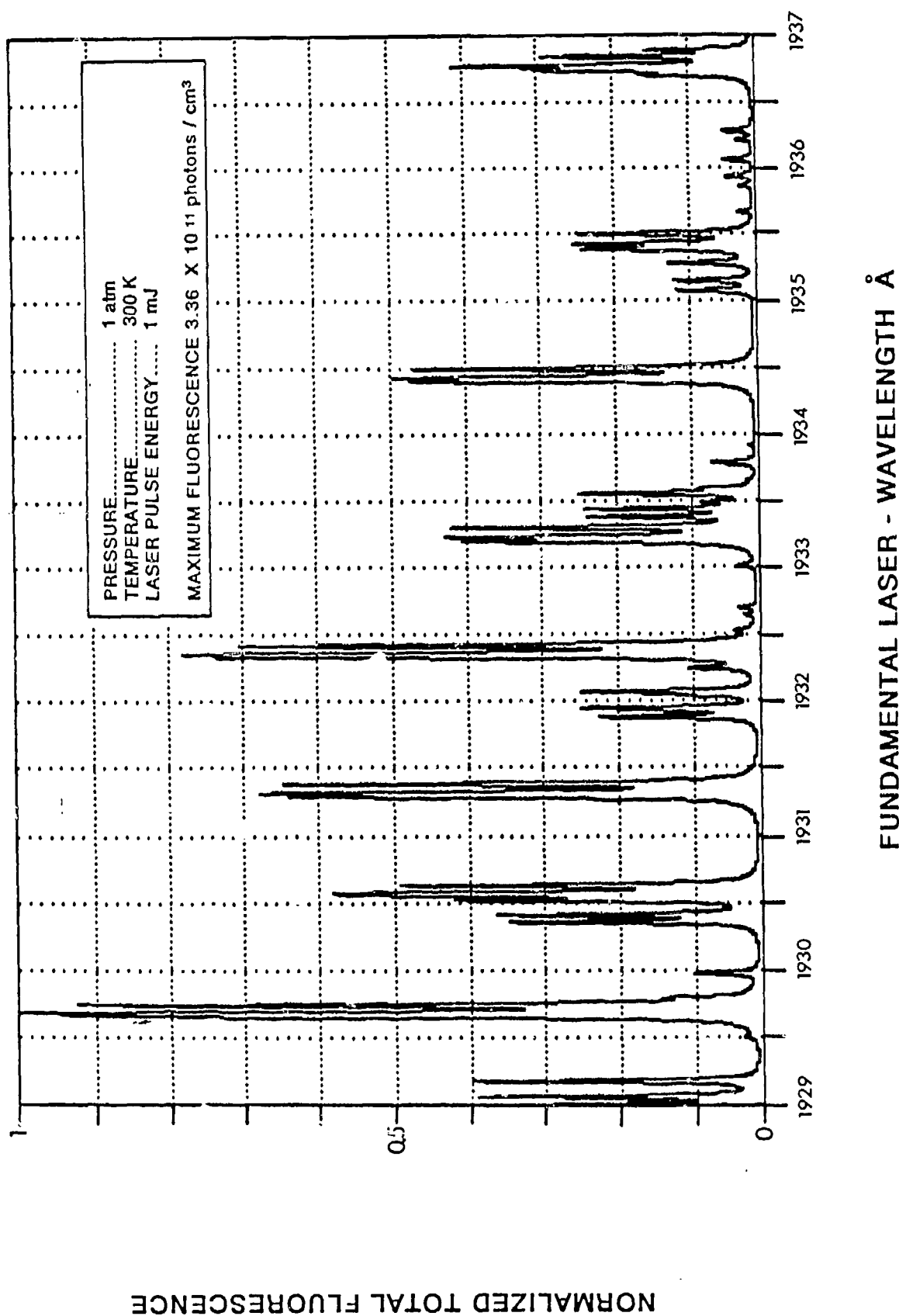
36

Fig.6. The calculated excitation spectrum of room air which is excited by a Raman shifted ArF laser at a wavelength of 179 nm, with a line width of 9 GHz and an energy of 1 mJ/pulse.

37

This transmission function simulates the filtration which is necessary for the removal of the radiation which is scattered at the the laser frequency and of fluorescence which may be induced by the wind tunnel windows. The abscissa is marked with the fundamental wavelengths of the laser. Most of the lines which can be observed in this spectrum are composed of overlapping transitions. Only the v'(0) to v'(13) R13 transition at 193.13 nm and the v''(0) to v'(13) P15 transition at 193.44 nm appear sufficiently isolated from the other transitions. However, even these transitions are composed of three fine structure lines which are due to the spin-orbit splitting. These lines are characterized by the total angular momentum J where:

$$
\begin{array}{ll}
I=1: & J=K-1 \\
I=2: & J=K \\
I=3: & J=K+1
\end{array}
\tag{28}
$$

and where K is the total quantum number apart from spin. Figure 7 presents the detailed spectrum of the P15 line. The observed structure is the convolution of the laser line with each of the fine structure absorption lines which are labeled by their I values. As a result of this convolution the I=2 line which is enclosed between the I=1 and I=3 lines appears stronger than the two other lines.

Figure 8 presents the variation with gas temperature of the total fluorescence which is observed following the selective excitation of each of the fine structure lines in the P15 transition. The maximum fluorescence is observed at 270 K. This is also the temperature at which the population of the ground state peaks. The temperature for maximum fluorescence for I=2 which is predicted by equation (18) is 249 K. The slight deviation from the the prediction of equation (18) can be attributed to the contribution to the total fluorescence of other transitions which coincide with the wings of the laser spectral distribution. An error of 1% in the prediction of the total fluorescence can account for an error of 10 K
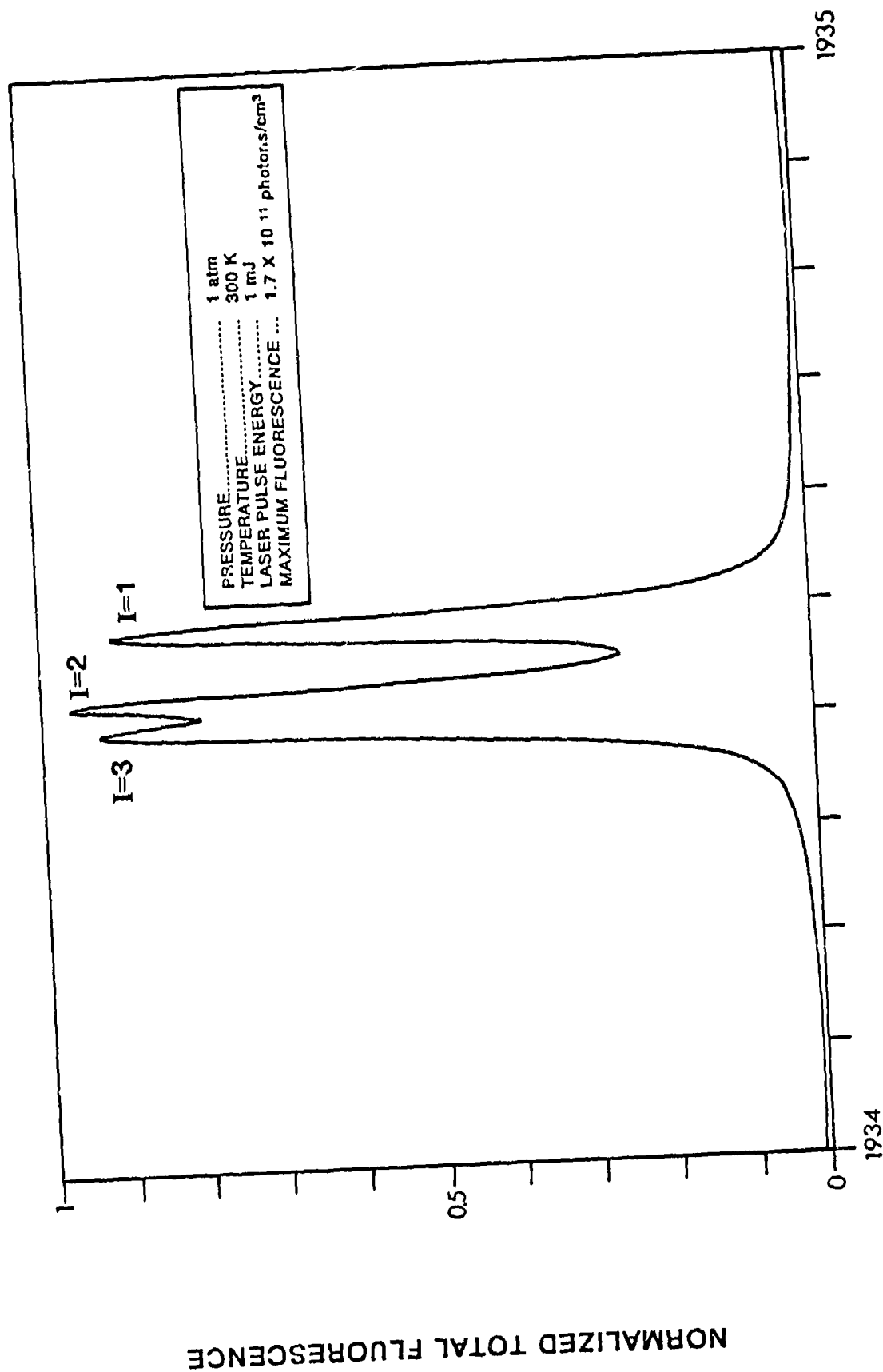
Fig.7. The detailed excitation spectrum of the $v''(0)—v'(13)$ P15 line. Laser parameters are as in figure 6.
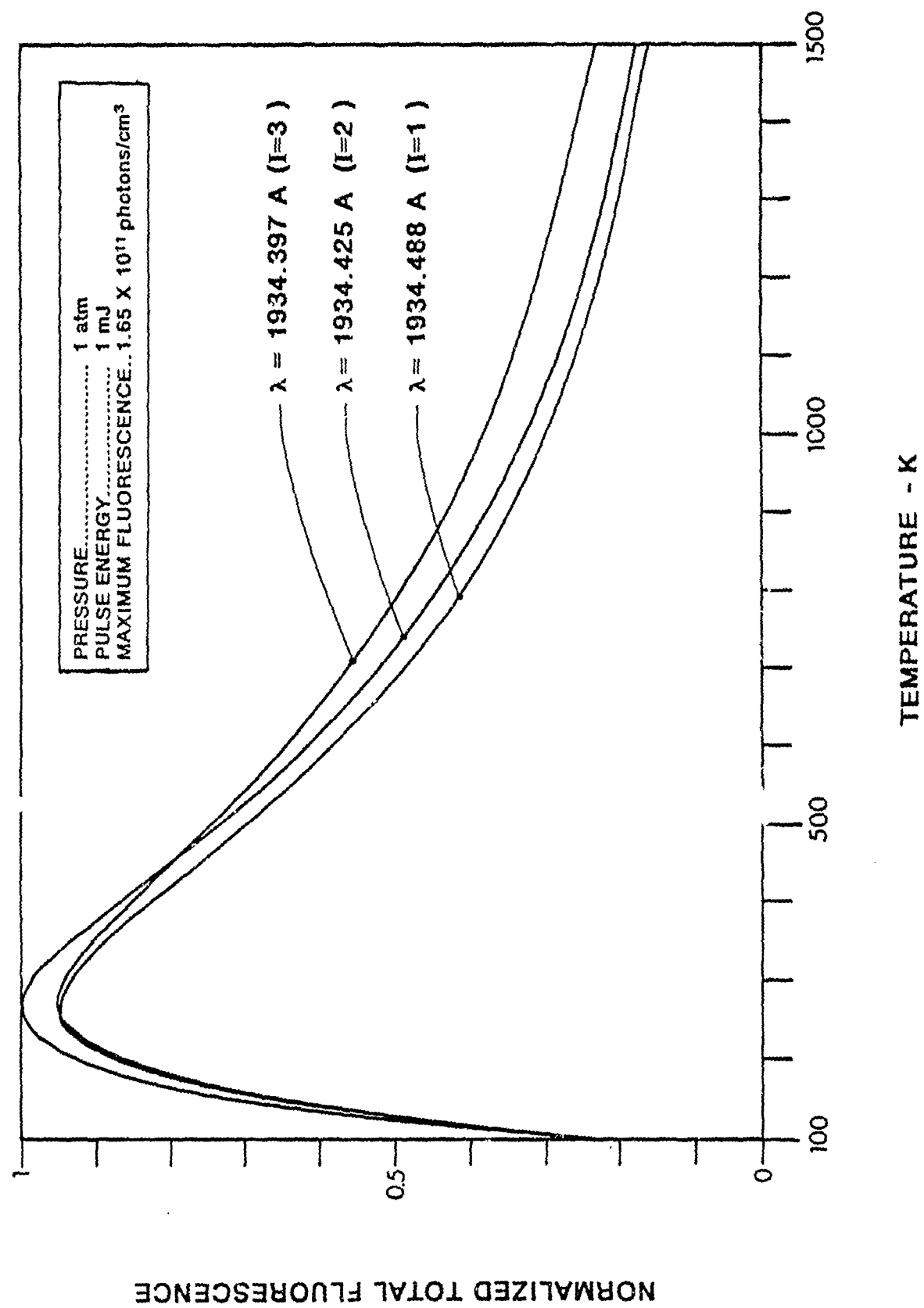
39

Fig.8. The variation with air-temperature of the total fluorescence which is observed following the selec-
tive excitation of each of the fine structure lines of the $v''(0)$–$v'(13)$ P15 transition.

The following appears within the figure:

PRESSURE.................... 1 atm
PULSE ENERGY.............. 1 mJ
MAXIMUM FLUORESCENCE..1.65 X 10^{11} photons/cm^3

$\lambda = 1934.397$ A (I=3)

$\lambda = 1934.425$ A (I=2)

$\lambda = 1934.488$ A (I=1)

TEMPERATURE - K

NORMALIZED TOTAL FLUORESCENCE

40

in the prediction of the temperature for maximum fluorescence. When the temperature is below 400 K, fluorescence emitted by the transition from $I=2$ is the highest. However, as temperature increases the intensity of the $v''(0)$ to $v'(17)$ P29 $I=1$ line which overlaps the $I=3$ line increases. As a result, the intensity of the fluorescence which is excited when the laser is tuned to the $I=3$ line increases faster than the intensity of the other two lines in the P15 manifold. When there is an overlap between two transitions which originate from two rotational levels with different N quantum numbers, the analysis of the temperature dependence of the fluorescence must include the contribution of both lines. Therefore, to simplify the analysis, only the R13 line, which does not overlap any other transition, should be used for these measurements.

Figure 9 presents the temperature dependence of the total fluorescence which is emitted when the laser is tuned to the $v''(0)$ $v'(13)$ R13 transitions. All the fine structure lines behave similarly. The temperature for maximum fluorescence when $I=1$ is lower than the temperature for maximum fluorescence for $I=3$. This is predicted by eqn.(18). It is seen from this figure that the curves which represent the three fine structure lines behave similarly. This indicates that the contribution of other transitions to the total fluorescence of each of the fine structure lines is negligible for all temperatures up to 1500 K.   W i t h the availability of a single absorbing line, the measurement technique will resemble the approach of Hiller et al.[16] and Hassa et al. [17]. The intensity of the fluorescence induced by the laser in molecules moving opposite to the beam will be subtracted from the fluorescence intensity induced in molecules moving in the direction of the beam propagation. In a typical Differential Intensity Measurement experiment, a laser pulse will be guided into the wind-tunnel at a slant angle with the axial flow direction. This allows detection of the Doppler shift associated with the main velocity component. After crossing the wind-tunnel and after a delay which exceeds the pulse duration, the beam will be retro-reflected. The delay is necessary for the separation of the fluorescence induced by the incoming beam from the
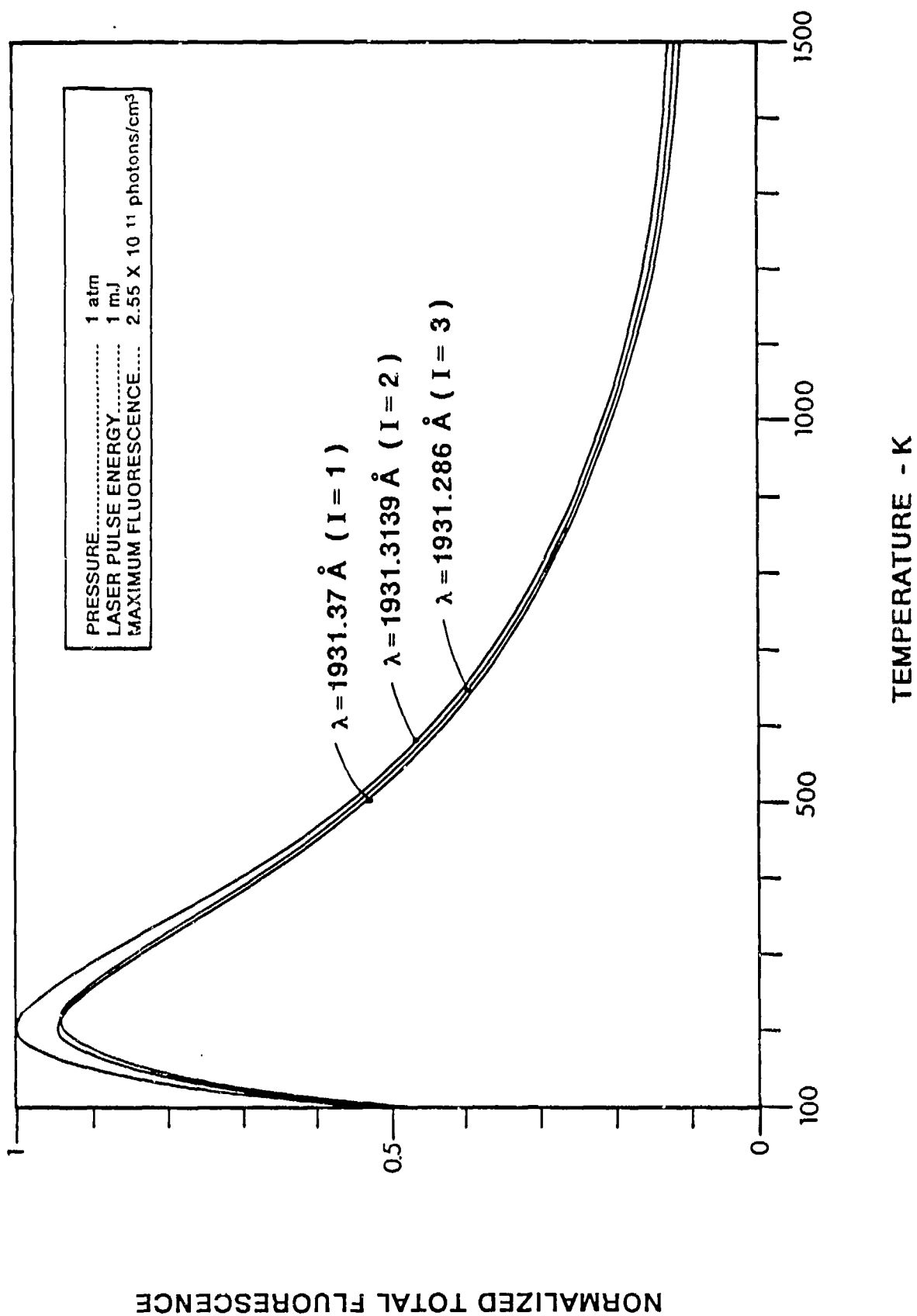
Fig.9. The variation with air-temperature of the total fluorescence which is observed following the selective excitation of each of the fine structure lines of the v"(0)-v'(13) R13 transitions.

42

fluorescence induced by the retro-reflected beam. The difference in intensity between the two fluorescence bursts can be related theoretically or experimentally [17] to the flow velocity. Figure 10 presents schematically the interaction of the laser beam with the R13 line. The laser is tuned to the short wavelength (high frequency) side of the $I=3$ line. The excitation spectra which are expected for the Doppler up-shifted and Doppler down-shifted frequencies were marked by the dashed lines. The intensity differences between the fluorescence induced by the Doppler up-shifted, the Doppler down-shifted and the un-shifted frequencies are evident in this figure.

Figure 11 presents the photon count difference, N_D, i.e. the difference between the fluorescence intensity following the excitation of the the $v''(0)$ to $v'(13)$ R13 transition by a laser beam which is propagating opposite to the flow and between the fluorescence which is excited by a laser which co-propagates with the flow, vs. the laser wavelength while the velocity is selected as a free parameter. The figure represents velocities ranging from 100 m/sec to 2000 m/sec in intervals of 100 m/sec. The upper velocity limit is approximately the highest air speed which can be obtained for a stagnation temperature of 1500 K. For each of the fine structure lines, the difference is negative when the laser is tuned to the high frequency side of the line and is positive when the laser is tuned to the low frequency side. This figure can be used to select the laser wavelength which will induce the FD which is the most sensitive to air velocity. The maximum difference is expected at the inflection point of the line. Therefore, two maxima are expected for each of the fine structure lines. The measurement of the difference in the fluorescence is most sensitive to the flow velocity when the laser is tuned to 193.1272 nm which is at the high frequency side of the $I=3$ line and when it is tuned to 193.1392 nm which is on the low frequency slope of the $I=1$ line. Tuning the laser to the center of a single absorption line will result in no velocity sensitivity.

43
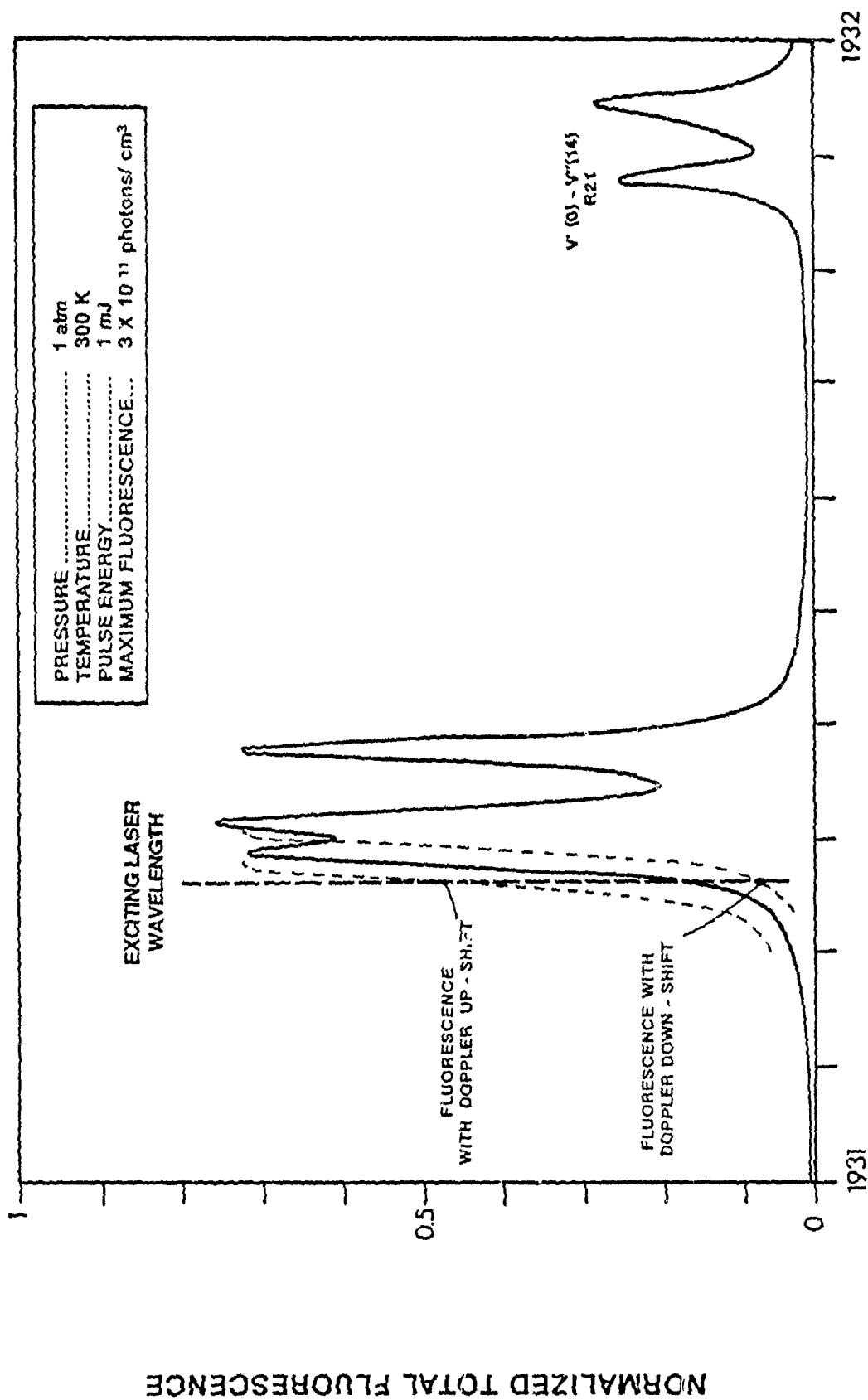
FUNDAMENTAL LASER - WAVELENGTH Å

Fig.10. Schematic presentation of the excitation spectrum of the $v''(0)-v'(13)$ R13 line. The short wavelength (high frequency) side of the I=3 line is marked by the vertical line. The excitation spectra which are expected for the Doppler up-shifted and Doppler down shifted frequencies were marked by the dashed lines.
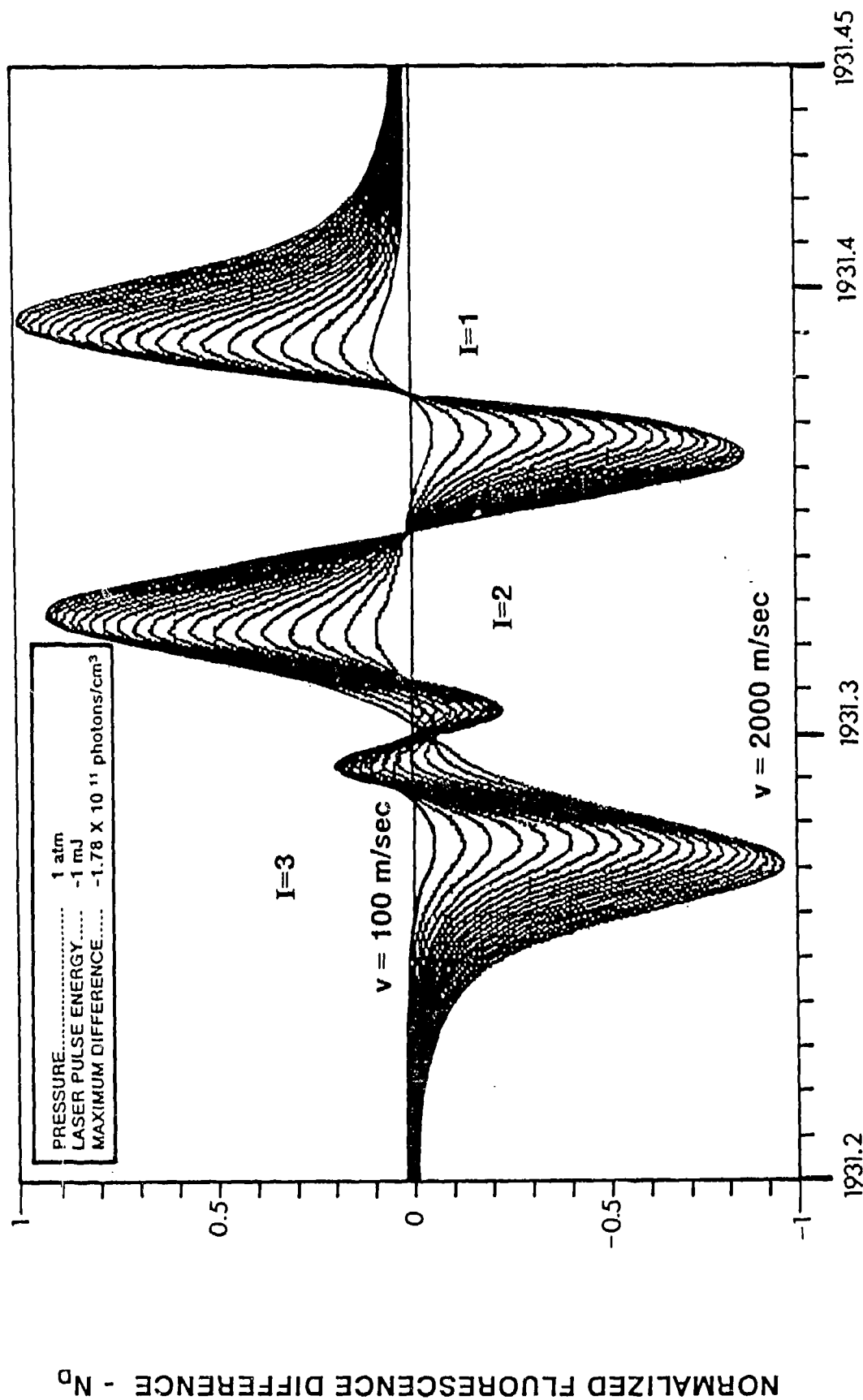
44

FUNDAMENTAL LASER WAVELENGTH - Å

NORMALIZED FLUORESCENCE DIFFERENCE - N_D

Fig.11. The photon count difference, N_D, following the excitation of the the $v''(0)$ to $v'(13)$ R13 transition vs. the laser wavelength while the velocity is selected as a free parameter. Velocities are ranging from 100 m/sec to 2000 m/sec in intervals of 100 m/sec.

3.2.2. The Effect of Temperature and Density on the Measurement Accuracy

The measurement of N_D is expected to vary with temperature and density very much like the variation of the total fluorescence (eqn. 17). Therefore, the measurement of the velocity using this technique must rely on the independent measurement of the temperature and the density.

The dependence of the FD measurement on temperature and density may be reduced by dividing the FD with the total fluorescence, Nc, induced in the absence of a Doppler shift. This signal contains the same temperature and density information as the FD but is independent of the flow velocity. This additional fluorescence measurement can be obtained by using a third laser beam which propagates perpendicularly to the flow. In cases where the slope of the wing of an absorption line can be approximated as a straight line, this correction of the FD will eliminate the temperature and density dependence. In most cases however, such an assumption may not be warranted and therefore, this correction is expected only to reduce the temperature and density effects on the FD signal.

The variation of N_D with velocity was calculated while selecting the temperature as a free parameter. The laser wavelength was $\lambda = 193.1272$ nm. This the the wavelength at the high frequency side of the R13/I3 line at which the velocity sensitivity is the highest. Figure 12 presents the results of this calculation for temperatures ranging from 100 K to 1500 K. This is the range of interest in most hypersonic wind tunnel applications. The count difference N_D in this figure increases with temperature when the gas temperature is below 250 K and than decreases as temperature increases. This is similar to the variation of the total fluorescence with temperature as predicted by figure 9. In addition, the slope of all curves decreases at high velocities. Therefore, the measurement sensitivity is expected to decrease as the air velocity approaches 2000 m/sec. It is apparent from this figure that the measurement of N_D can not be correlated with velocity without an independent measurement of the temperature. Furthermore, according to eqn.(17), the population of the ground state is
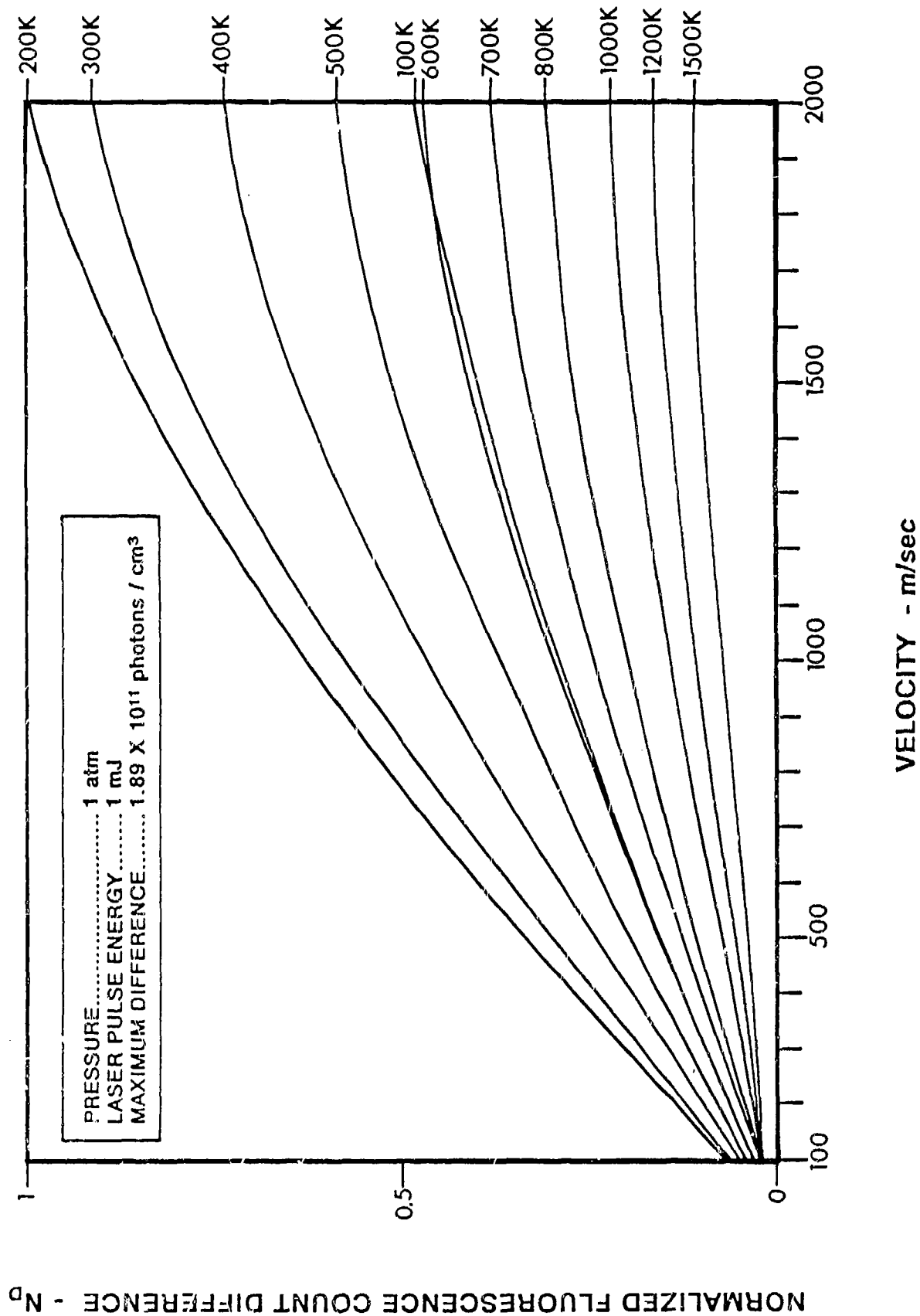
Fig.12. The variation of N_D with velocity for temperatures ranging from 100 K to 1500 K. The laser wavelength is $\lambda = 193.1272$ nm.

47

proportional to the total density and the absorption cross-section varies with pressure due to the pressure broadening. Therefore, N_D also varies with density or pressure and the velocity measurement must also include a separate density measurement. As a result, the uncertainty in the measurement of the velocity will be affected by the uncertainties in the measurements of the density and the temperature.

To evaluate the effectiveness of the temperature and density correction technique, we repeated the calculation of the FD and used the total fluorescence induced by the unshifted beam for normalization. Figure (13) presents the variation with velocity of the temperature and density corrected FD, $\bar{N}_D = N_D / N_c$. Several temperatures were selected as free parameters while the pressure was kept constant at 1 atmosphere. The other conditions for this calculation are identical to those described for figure (12). This calculation presents the temperature dependence of the corrected FD. It is seen that for low temperature, when the contribution of both the pressure and temperature broadening to the total line width varies rapidly the corrected FD is sensitive to temperature. However, above 500K the corrected FD is nearly independent of temperature. This strong temperature dependence below 500 K was attributed to the rapid changes in the pressure and Doppler broadening (eqns. (13) and (14)). While the pressure line-width decreases with the temperature the Doppler line-width increases. Above 500 K, The sum of these two mechanisms was almost independent of temperature. This is where the temperature correction becomes effective.

To evaluate the density dependence of the corrected FD we repeated the calculation with the pressure as the free parameter. Figure 14 presents the variation with velocity of the temperature and density corrected FD. Here the temperature was kept at 100K. The sensitivity of the FD to pressure was found to be the greatest at this temperature. It is seen
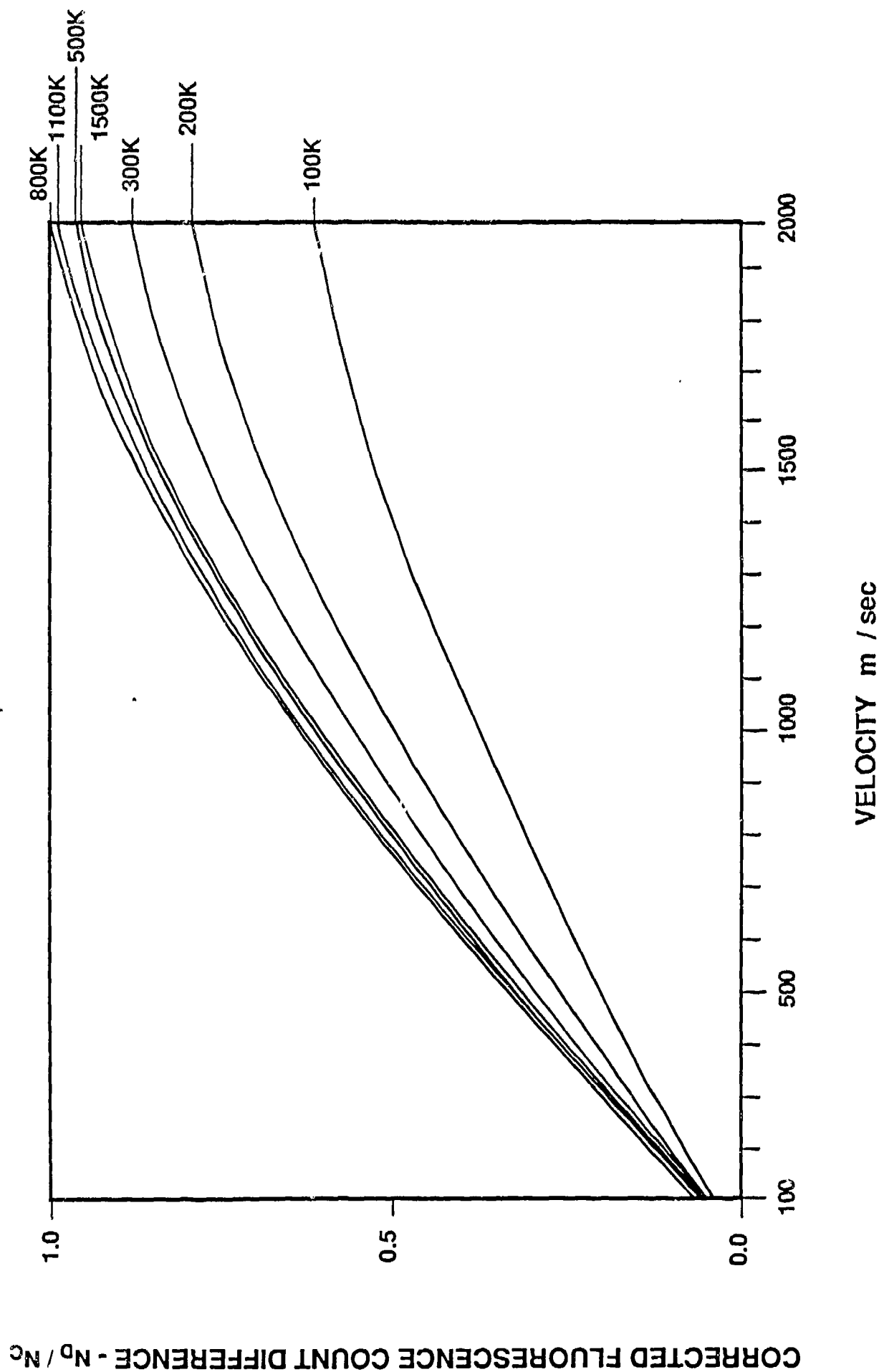
48

Fig.13. Temperature and density corrected FD, $N_D = N_D/N_c$, vs. velocity. The temperatures which were selected as free parameters are indicated in the figure, the pressure is 1 atmosphere and the laser wavelength is $\lambda = 193.1272$ nm.
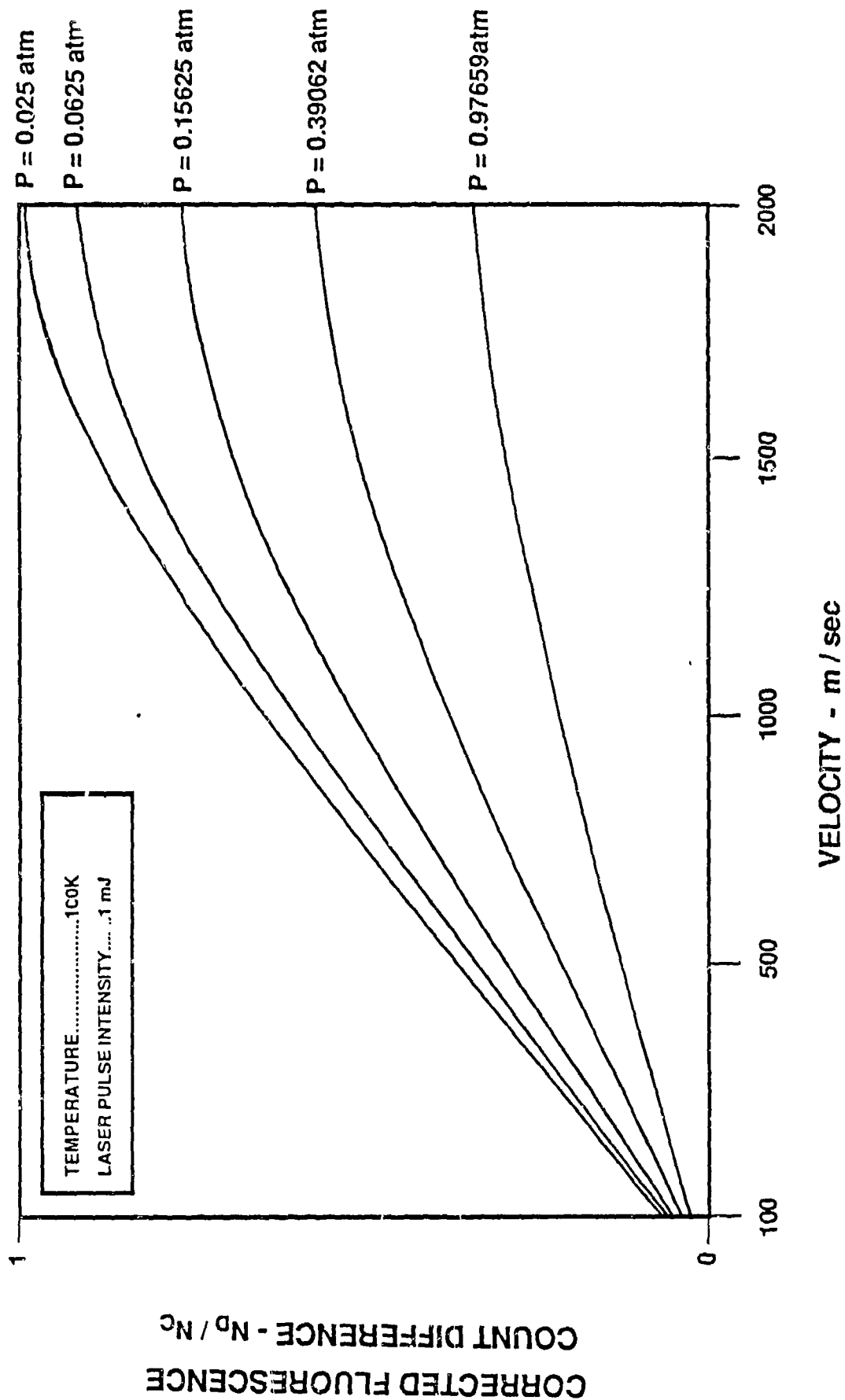
VELOCITY m / sec

CORRECTED FLUORESCENCE COUNT DIFFERENCE - N_D / N_C

Fig.14. Temperature and density corrected FD, $N_D = N_D/N_c$, vs. velocity. The pressures which were selected as free parameters are indicated in the figure, the temperature is 100k and the laser wavelength is $\lambda = 193.1272$ nm.

P = 0.025 atm

P = 0.0625 atm

P = 0.15625 atm

P = 0.39062 atm

P = 0.97659atm

VELOCITY - m / sec

CORRECTED FLUORESCENCE
COUNT DIFFERENCE - N_D / N_C

TEMPERATURE...........1C0K
LASER PULSE INTENSITY.....1 mJ

50

that although the FD has been corrected by the normalization it still presents a strong density dependence. The error term $(\partial N_D/\partial\rho)_{V,T}\Delta\rho$ which is introduced into the velocity measurement due to uncertainty in the density measurement was found to increase with density. Again, the increasing pressure line-width was found to be the cause for the density dependence of the corrected FD.

In a previous work [2], we determined the uncertainty which is associated with the measurement of the temperature and density in hypersonic wind tunnel air flows using an LIF and Raman technique and assuming that the measurement will be limited by the photon-statistical noise. The uncertainty in the temperature measurement, $\Delta T/T$, when the air density is 0.01 amagat and the laser energy at 193.4 nm is 15 mJ/pulse was found to be less than 0.5%. The uncertainty in the density measurement, $\Delta\rho/\rho$, using a 15 mJ pulse to excite Raman scattering from 0.01 amagat of air was found to be less than 2.7%. This is however a conservative estimate. The pulse energy at 193.4 nm in most applications may exceed 100 mJ. Therefore, the uncertainty in the density measurement is expected to be less than 1%. The model may now be applied to estimate the uncertainty with which velocity can be measured using an achievable laser performance at the gasdynamic conditions of interest. Examples calculated using Eq. (27) are based on the assumption that photon-statistical noise is the limiting cause for the uncertainty in the velocity measurement. However, we shall also show examples in which the minimum Noise to Signal Ratio (NSR) is limited to 1% to simulate the case where the noise is induced by Electromagnetic effects or by digitization. The uncertainty of an LIF temperature measurement was calculated using Eq.(27) for gas pressures of .01 atmospheres and temperatures varying from 100 K to 1500 K. This covers the range of most applications. For example, at a free-stream Mach number of 10, a total pressure of 100 atm., and a total temperature of 1000 K, the flow field over a typical hypersonic aerodynamic body has densities which vary from 0.01 to 0.05 amagat and temperatures from 50 to 250 K. The stagnation temperature however, may

approach 1000 K. The calculations were made assuming that the Raman shifted laser pulse energy is 1 mJ, with fluorescence and Raman scattering observed from a 1-mm beam path with f/2 collection optics and a detector with 15% quantum efficiency. These optical conditions are equivalent to a laser fluence of .1 J/cm^2 in a sample volume with a beam cross-section of 1 mm^2. The uncertainty in the temperature measurement was assumed to be .05% and the limiting uncertainty in the density measurement was assumed to be 1%. The density error term $(\partial N_D/\partial \rho)_{v,T} \Delta \rho$ was evaluated using the calculation of fig. (14) for P = 1 atm and T = 100 K. This is the largest error in this range. The temperature error term was calculated separately for each temperature.

The results are shown in figure (15) for the laser tuned to the high frequency slope of the I3/R13 rotational transition in the v"(0) - v'(4) vibrational band. The solid line is based on the assumptions that the uncertainty in the velocity measurement is composed of the uncertainty in the temperature and density measurements. However, unlike the assumptions in eqn.27 the uncertainty in the FD was assumed to be limited to 1%. Therefore, the solid line presents the most conservative estimate of the measurement uncertainty. It indicates however that at the most adverse conditions the measurement uncertainty may be kept below 10%. The next estimate presents the uncertainty associated with a velocity measurement using the temperature and density corrections technique. Here, the uncertainty can be kept below 5%. The dotted line shows the results if the minimum NSR in the FD is limited to 1% by EMI or other noise sources but the temperature and density are determined precisely. This presents the uncertainty in the velocity measurement which may be obtained in some experimental conditions. Finally, the dashed line presents the measurement uncertainty when the FD is limited by the shot noise and the temperature and density are determined precisely. This curve presents the physical limit for the velocity measurement uncertainty using this Doppler velocimetry technique. It is seen that the accuracy of the velocity measurement using O_2 as the tracer molecule can not exceed 0.1%
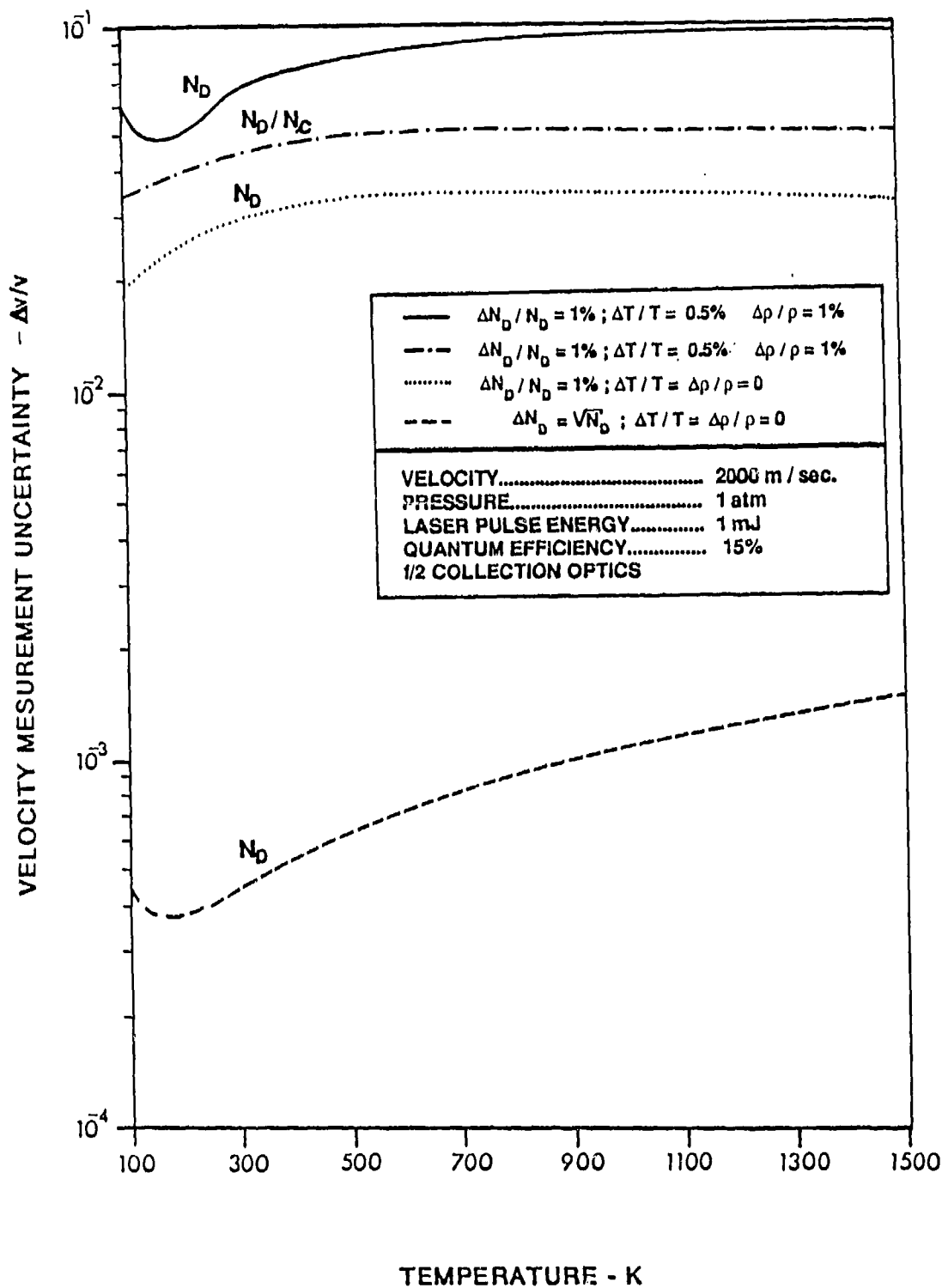
52

Fig.15. Velocity measurement uncertainty $\Delta v/v$ vs. temperature for the laser tuned to the $v'(0)-v'(13)$ R13 transition. The solid line presents the total uncertainty which is composed of the uncertainty in the temperature and density measurements and $\Delta N_D/N_D = 1\%$. The (-·-·) presents the uncertainty when using the temperature and density corrections. The dotted line presents the uncertainty when the only error is $\Delta N_D/N_D = 1\%$. The dashed line presents the measurement uncertainty when the only error is $N_D = \sqrt{N_D}$.

53

4. CONCLUSIONS

A new velocimetry technique which uses a single pulse from an ArF laser for the generation and the subsequent detection of CO tracers was analyzed theoretically and experimentally. The intensity emitted by fluorescing carbon atoms, which are the dissociation products of atmospheric CO_2, was expected to be sensitive to air velocity.

An alternative technique which uses the Doppler shift experienced by moving O_2 molecules for the measurement of their velocity was evaluated theoretically. The Doppler shift is measured by using a differential intensity measurement technique. In this approach two counter-propagating laser beams are tuned to the high frequency wing of one of the absorption lines of O_2 molecules within the air flow. In the absence of flow, both beams encounter the same absorption cross-section and induce the same fluorescence intensity. However, when the absorbing molecules are moving along the laser beams together with the gas flow, the absorbed radiation is Doppler shifted: the frequency of the radiation of the beam which propagates opposite to the flow is Doppler up-shifted and is therefore further away from the absorption line-center. Therefore, fluorescence intensity induced in molecules which move opposite to the beam decreases. The other laser beam - which propagates in the direction of the N_2 flow - is experienced by the moving molecules as Doppler down-shifted. Therefore, the fluorescence induced by this beam will be more intense. The difference between the intensities of these two LIF processes is sensitive to the air speed.

The results of our study yielded the following conclusions:

- When the air temperature is below 2000 K and the pressure is between 0.01 atmosphere and 10 atmospheres the fluorescence emitted by the dissociation products of CO_2 is independent of temperature. Above this temperature the equilibrium density of CO_2 decreases rapidly.

- The total fluorescence emitted by the dissociation products of CO_2 strongly depends on the energy distribution across the laser beam. Fluctuation in the energy distribution may introduce an uncertainty in the velocity measurement of up to 40%.

- A preliminary experiment tested the sensitivity of the total fluorescence which is induced by an ArF laser in the dissociation products of CO_2 to supersonic flows. No variation in the total fluorescence could be detected for air speeds up to Mach 2.2. It is believed that multiphoton ionization and quenching processes interrupt the photodissociation of CO_2 and CO and the LIF process.

- The $v''(0) - v'(13)$ R13 transition is the only line which is resonant with the Raman shifted ArF laser and is also isolated from other absorption lines in the Schumann-Runge band.

- It was shown theoretically that even if the FD signal is normalized by the total fluorescence which is emitted by stationary molecules the normalized signal still presents a strong density and temperature dependence.

- When the FD signal is not corrected for density and temperature, the uncertainty in the velocity measurement for all temperatures below 1500 K and for densities below 1 atmosphere is less than 10%.

- When the FD signal is normalized by the total fluorescence emitted by stationary molecules the uncertainty in the velocity measurement for all temperatures below 1500 K and densities below 1 atmosphere is less than 5%.

- The ultimate accuracy of this Doppler velocimetry technique is obtained when the temperature and density are accurately known and when the fluorescence is measured within an uncertainty which is limited by the shot-noise. The uncertainty in the velocity measurement is than less than 0.1%.

5. RECOMMENDATIONS

1. The single pulse carbon velocimetry did not appear to have the necessary sensitivity to air speed. Therefore, we do not recommend its application for wind tunnel diagnostics.

2. We recommend the application of the Doppler velocimetry in oxygen for wind tunnel diagnostics.

3. We recommend to use the Fluorescence Difference (FD) approach for single pulse velocity measurements.

4. We recommend to use the absorption in the $v''(0)$-$v'(13)$ R13 transition for these velocity measurements.

5. We recommend to normalize the FD signal by the total fluorescence induced in stationary molecules. This normalization will reduce the temperature and density dependence of the FD measurement.

6. REFERENCES

1. G.Laufer and R.L.McKenzie, "Radiative Processes in Air Excited by an ArF Laser.", Opt.Lett., Vol.13, No.2, p.99-101,1988

2. G.Laufer and R.L.McKenzie, Temperature Measurements in Hypersonic Air Flows Using Laser-Induced O_2 Fluorescence, AIAA/NASA/AFWAL Conference on Sensors and Measurement Techniques for Aeronautical Applications, AIAA-88-4679-CP, Atlanta, G.A,1988.

3. G.Laufer, Development of an Integrated System for the Wind Tunnel Measurement of Air Temperature and Density. DARPA Contract #DAAH01 87 C 0847, Final Report, January 1988.

4. B.A.Thompson,P.Harteck, and R.R.Reeves,Jr., "Ultraviolet Absorption Coefficient of CO_2, CO, O_2, H_2O, N_2O, NH_3, NO, SO_2, and CH_4 Between 1850 and 4000 A.", J.Geo.Res., Vol.68, No.24, P.6431-6436, 1963.
   also
   P.Hartek,R.R.Reeves,Jr., and B.A.Thompson, "Photochemical Problems of the Venus Atmosphere.", NASA Technical Note, D-1984, 1963.

5. J.Bokor, J.Zavelovich and C.K.Rhodes, "Isotope Effect in Multiphoton Ultraviolet Photolysis of CO", J.Chem.Phys., Vol.72, No.2, P.965-971, 1980.

6. W.K.Bischel, J.F.Bokor, D.J.Kligler, and C.K.Rhodes, "Nonlinear Optical Processes in Atoms and Molecules Using Rare-Gas Halide Lasers", IEEE J.Quant.Elect., Vol.QE-15, No.5, P.380-392, 1979.

7. W.L.Weiss, M.W.Smith, and B.M.Glennon, "Atomic Transition Probabilities", Vol.1, National Standard Reference Data Series, NSRDS-NBS 4, 1966.

8. R.W.B. Pearse, and A.G.Gaydon, "The Identification of Molecular Spectra", Chapman and Hall, 1976.

9. J.Haumann,J.M.Seitzman, and R.K.Hanson, "Two-Photon Digital Imaging of CO in Combustion Flows Using Planar Laser-Induced Fluorescence", Opt.Lett., Vol.11, P.776-778, 1986.

10. P.A.Thompson, Compressible-Fluid Dynamics, McGraw-Hill, 1977.

11. J.W.Goodman,Introduction to Fourier Optics, McGraw-Hill, 1968.

12. D.A.Anderson, J.C.Tannehill, R.H.Pletcher, Computational Fluid Mechanics and Heat Transfer, McGraw-Hill, 1984.

13. M.Zimmermann and R.B.Miles, "Hypersonic-Helium-Flow-Field Measurements with the resonant Doppler Velocimeter.", App.Phys. Lett., Vol.37, No.10,P.888-887,1980.

14. C.Y.She, W.M.Fairbank,JR., and R.J.Exton, "Measuring Molecular Flows with high-Resolution Stimulated Raman Spectroscopy", IEEE J.Quant.Elect., Vol.QE-17, No.1, P.2-4, 1981.

15. R.J.Exton, M.E.Hilliard, W.R.Lempert, P.F.Covell and D.S. Miller, "molecular Flow Velocity Using Doppler Shifted Raman Spectroscopy", AIAA 22nd Thermophysics Conference, Hawaii, AIAA-87-1531, June 8-10, 1987.

16. B.Hiller,J.C.McDaniel,E.C.Rea, Jr and R.K.Hanson, "Laser-Induced Fluorescence Technique for Velocity Field Measurement in Subsonic Gas Flows." Opt.Lett., Vol.8, No.9, pp 474-476,1983.

17. C.Hassa, P.H.Paul, and R.K.Hanson, "Laser Induced Fluorescence Modulation Technique for Velocity Measurements in Gas Flows", Exp.in Fluids, Vol.5, P.240-246, 1987.

18. P.H.Krupenie, "The Spectrum of Molecular Oxygen", J.Phys.Chem. Ref.Data., Vol.1, No.2, P.423-534, 1972.

19. B.Ruckle, P.Lokai, U.Brinkmann, D.Basting, W.Muckenheim, "Tunning Ranges of an Injection Locked Excimer Laser", Opt. and Laser Tech., Vol.19, No.3, P.153-157, 1987.

20. B.R.Lewis,L.Berzins,J.H.Carver and S.T.Gibson, "Rotational Variation of Predissociation Linewidth in the Schumann-Runge Bands of $^{16}O_2$", J.Quant.Spectrosc.Radiat.Transfer., Vol.36, No.3, pp.187-207, 1986.

21. A.Yariv, "Quantum Electronics", John Wiley & Sons, 1975. 22.R.Vehrenkamp, "Generation of Tunable VUV-Radiation by Powerful Excimer/Dye Laser Systems", Lambda Physik Technical Notes, 1987.

23. A. S. C. Cheung, K. Yoshino, W. H. Parkinson, and D. E. Freeman, J. Molec. Spectrosc., 119, 1, (1986).

24. L. Veseth and A. Lofthus, "Fine Structure and Centrifugal Distortion in the Electronic and Microwave Spectra of O2 and SO",Molecular Physics, vol.27, No.2, p.511-519, 1974.

25. K. Yoshino, D. E. Freeman, and W. H. Parkinson, "Atlas of the Scumann-Runge Absorption Bands of O2 in the Wavelength Region 175-205 nm", J. Phys. Chem. Ref. Data, vol.13, No.1, p.207-227, 1984.

26. Y. Endo and M. Mizushima, "Microwave Resonance Lines of $^{16}O_2$ in its Electronic Ground State ($X^3\Sigma_g^-$), Jap.J.of App. Phys., vol.21, No.6, p.L379-L380, 1982.

27. W. M. Huo and C. W. Bauschlicher, Jr., 8th Annual West Coast Theoretical Chemistry Conference, paper TP8, March 26, (1986).

28. K. Yoshino, D. E. Freeman, J. R. Esmond, and W. H. Parkinson, Planet Space Sci., 31, 339, (1983).

29. M. W. P. Cann, R. W. Nicholls, W. F. J. Evans, J. L. Kohl, R.Kurucz, W.H. Parkinson and E. M. Reeves, Appl.Opt., 18, 964, (1979).

30. A.Comey, "Atomic Laser Spectroscopy", Clarendon Press, Oxford, 1977.

31. G.Herzberg,"Molecular Spectra and Molecular Structure,I,Spectra of Diatomic Molecules", Van Nostrand Co.,1950.

32. H. A. Gebbie, W. J. Burroughs, J. A. Robb, and G. R. Bird, Nature, 212, 66, (1966).

33. D. Marcuse, Engineering Quantum Electrodynamics, Harcourt, Brace, and World, Inc., New York, (1970).